AD-A035 348 TORONTO UNIV (ONTARIO) INST FOR AEROSPACE STUDIES F/G 7/4
CONDENSATION OF WATER VAPOUR ON HETEROGENEOUS NUCLEI IN A SHOCK--ETC(U)
APR 76 S KOTAKE, I I GLASS AF-AFOSR-2274-72

UNCLASSIFIED UTIAS-207 AFOSR-TR-77-0039 NL

| OF |
AD
A035348

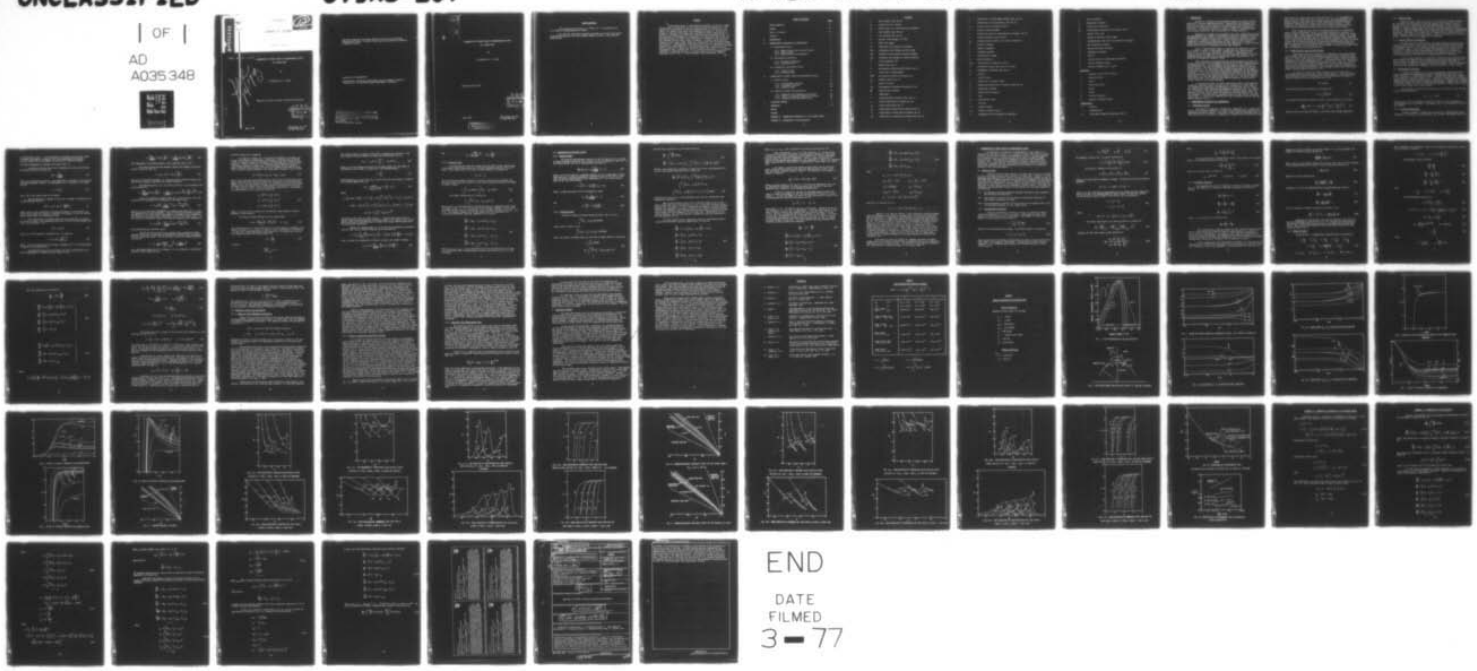

END

DATE
FILMED
3-77

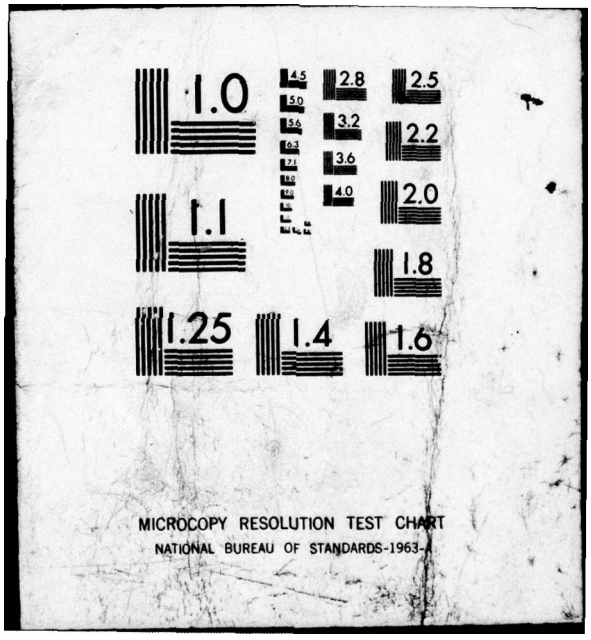
1.0
1.1
1.25
1.4
1.6
1.8
2.0
2.2
2.5
2.8
3.2
3.6
4.0
4.5
5.0
5.6
6.3
MICROCOPY RESOLUTION TEST CHART
NATIONAL BUREAU OF STANDARDS-1963-A

INSTITUTE
FOR
AEROSPACE STUDIES

UNIVERSITY OF TORONTO

AFOSR - TR 77 - 0039

CONDENSATION OF WATER VAPOUR ON HETEROGENEOUS NUCLEI IN A SHOCK TUBE

by

S. Kotake and I. I. Glass

April 1976

UTIAS Report No. 207
CN ISSN 0082-5255

Qualified requestors may obtain additional copies from the Defense Documentation Center, all others should apply to the National Technical Information Service.

Conditions of Reproduction:

Reproduction, translation, publication, use and disposal in whole or in part by or for the United States Government is permitted.

AIR FORCE OFFICE OF SCIENTIFIC RESEARCH (AFSC)
NOTICE OF TRANSMITTAL TO DDC
This technical report has been reviewed and is approved for public release IAW AFR 190-12 (7b).
Distribution is unlimited.
A. D. BLOSE
Technical Information Officer

CONDENSATION OF WATER VAPOUR ON HETEROGENEOUS NUCLEI IN A SHOCK TUBE

by

S. Kotake and I. I. Glass

Submitted March 1976

April 1976

UTIAS Report No. 207
CN ISSN 0082-5255

Acknowledgements

The discussions with Prof. D. S. Scott, Dr. J. P. Sislian and Dr. S. P. Kalra are acknowledged with thanks.

The work was financially supported by UTIAS and the Air Force Office of Scientific Research, Air Force Systems Command, U.S.A.F., under Grant No. AFOSR 72-2274.

Summary

A macroscopic model of heterogeneous nucleation is used for a theoretical study of condensation of water-vapour/carrier-gas mixtures in a non-equilibrium nonstationary rarefaction wave generated in a shock tube. The results are compared with those from homogeneous nucleation. Nucleation is assumed to take place heterogeneously on idealized smooth, spherical solid particles of Aitken nuclei, which are chemically and electrically inert. In the processes of heterogeneous condensation, the controlling factors are the size-distribution of nuclei, the concentration of monomers on the surface of the substrate and the contact angle of embryos. Of these factors the most dominant is the contact angle, which can reduce greatly the activation energy of nucleation. Heterogeneous condensation results in less supercooling of the mixture but a faster approach to the equilibrium state. By choosing a suitable value for the contact angle, the numerical results can be made to fit the experimental data. Although this is not entirely satisfactory, it is probably preferable to changing the value of surface tension as in the homogeneous nucleation case in order to obtain agreement with experimental results.

TABLE OF CONTENTS

Notation

A	rate variable, Eqs. 28, 36
A_o	surface area of a nucleus
A_s	surface area of a nucleus wetted by droplets
B	rate variable, Eqs. 28, 36
C	rate variable, Eqs. 28, 36
E	specific total energy $(e + u^2/2)$
G	Gibbs free energy
ΔG	activation free energy for nucleation
ΔG_b	condensation free energy per unit volume
ΔG_d	desorption free energy of adsorbed monomer
ΔG_s	activation free energy for surface diffusion
$\dot{I}$	total nucleation rate
J	monomer flux, Eq. 5
K	heterogeneous droplet growth factor, Eq. 32
L	latent heat of vaporization
$N(R)$	distribution function of nuclei, Eq. 1
N_A	Avogadro number, Eq. 74
R	radius of nuclei
R_H	heterogeneous nucleation constant, Eq. 24
$\mathcal{R}$	universal gas constant
T	temperature
Z	nonequilibrium correction factor, Eq. 15
a	volume coefficient of droplet, Eq. A-1
a_f	frozen sound speed, Eq. 47
a_s	liquid-solid surface area of droplet, Eq. 17
a_v	liquid-vapour surface area of droplet, Eq. 17
b_s	coefficient of liquid-solid surface area, Eq. A-2

b_v	coefficient of liquid-vapour surface area, Eq. A-3
c	coefficients in rate equations, Eqs. 28, 36
c_p	specific heat at constant pressure
e	specific internal energy
f	geometrical factor for heterogeneous nucleation, Eq. 23
g	overall condensate mass fraction
g_R	condensate mass fraction on a nucleus of radius R
h	specific enthalpy
i	number of monomers
k	Boltzmann constant
ℓ	characteristic length
m	mass of monomers
n(i)	concentration of embryos of size i
$\dot{n}$	nucleation rate per unit area of a nucleus
$\dot{n}_o$	homogeneous nucleation rate, Eq. 25
p	pressure
r	droplet radius
$\dot{r}$	growth rate of droplet radius
$\dot{r}_o$	homogeneous growth rate of droplet radius, Eq. 31
r_r	dimensional constant
s	supersaturation (p_v/p_s)
t	time
t_r	characteristic time
u	velocity
v	specific volume
v_ℓ	volume of droplet, Eq. 17
w	impingement rate of monomers on substrate

x	space coordinate
y	Lagrangian coordinate
α	condensation coefficient
β_d	nondimensional adsorption free energy, Eq. 24
γ	specific heat ratio
θ	embryo-to-substrate contact angle
λ	nondimensional latent heat of evaporation ($L/C_{p_o}T_o$)
μ	Lax dissipation constant
ν	adatom vibrational frequency
ξ	Lagrangian coordinate
ρ	density
σ	surface tension on liquid-vapour interface
φ	relative humidity (p_v/p_s)
ω	specific humidity $[(\rho_v + \rho_s)/\rho]$

Subscripts

o	condition in the driver section
s	saturation state
v	vapour
i	inert carrier gas
f	frozen
ℓ	liquid
R	nucleus of radius R
∞	nucleus of infinite radius

Superscripts

*	critical
-	nondimensional
< >	size-number weighted integration, Table 1

1. INTRODUCTION

Problems of two-phase and two-component systems have great practical importance in various engineering fields. Researches on the nucleation and growth by condensation and evaporation of droplets have been conducted over a long period of time and many aspects of these processes can be regarded as understood. Nevertheless, there still remains a number of unsolved problems such as phase transitions under the existence of foreign particles.

Homogeneous nucleation and condensation have been studied theoretically and experimentally by a number of investigators within the framework of one- or two-dimensional supersonic-nozzle flows and nonstationary rarefaction flows in a shock tube. Recently, Sislian (Ref. 1) made a detailed numerical study of homogeneous nucleation and condensation of water vapour with or without a carrier gas in the nonstationary rarefaction wave generated in a shock tube and predicted the effects of condensation on the flow variables.

Unless a supersaturated vapour is specially and expensively treated, it is likely to contain a large number of small particles (Aitken nuclei), which can act as nuclei of spontaneous condensation. Depending upon the cooling rate and the number of nuclei, the resulting phase change of the supersaturated vapour can take place at considerably lower supersaturation than predicted by homogeneous nucleation alone.

Since nucleation on foreign particles involves additional degrees of freedom, the analysis of heterogeneous nucleation is much more complicated than the homogeneous case. The nucleation rate will depend on the nature of the nucleus surface, including its geometry and physical and chemical properties. It also depends on the condition of the surface and the state of the vapour. Nevertheless, there are many similarities between homogeneous and heterogeneous nucleation. Due to these features, heterogeneous nucleation has been studied from both macroscopic and microscopic points of view, such as the capillarity model (Refs. 2, 6) and the small-cluster model (Ref. 3). The latter requires fairly microscopic data of physical and chemical properties of the nucleus surface which are not readily available.

In the present report, by using a macroscopic model of heterogeneous nucleation, numerical studies are made of the condensation of water vapour in the nonstationary rarefaction wave generated in a shock tube and the results are compared with those obtained from homogeneous nucleation (Ref. 1). Nucleation is assumed to take place heterogeneously on idealized smooth, spherical particles of Aitken nuclei, which are chemically and electrically inert. The flow variables in a shock tube are assumed to have the same initial conditions used in Ref. 1. The new flow properties are then calculated using the same Lax method employed in Ref. 1.

2. HETEROGENEOUS NUCLEATION AND CONDENSATION

2.1 Condensation Nuclei

As a source of commercial nitrogen gas, atmospheric air is widely used. The air has sufficient quantities of nuclei produced by physical, chemical and mechanical processes in nature. According to cloud physics terminology (Ref. 4), these particles are classified by dimension as, Aitken nuclei for particles with

radii below 0.1μ; large nuclei for those with radii 0.1 ~ 1μ; and gigantic or giant nuclei for those with radii in excess of 1μ. Large and gigantic nuclei usually contain a large quantity of soluble substances, primarily ammonium sulfate and sodium chloride. They are the most active of nuclei in cloud formation. The majority of Aitken nuclei are too small to become active in meteorological condensation provided they are not electrically charged.

Even cleaned air with careful filtration might carry a considerable number of these condensation nuclei. In industrial processes, the gases are passed through various pieces of equipment, heat exchangers, condensers, liquid-sprayed columns, contact apparatus with catalyst layers and filters. The number density of particles and their physical and chemical properties thus depend not only on those in the initial gas but also on the processing of the gas. By taking special care of physical filtration and electrical neutralization, large and gigantic particles and electrically charged particles can be excluded from the gas. Consequently, the processed gas can be assumed to contain only Aitken nuclei that are chemically and electrically inert.

2.1.1 Number Density and Size Distribution

Concentration and size distribution of atmospheric nuclei vary greatly with locality. The particles in greatest concentration are the Aitken nuclei, which are counted in the conventional Aitken nucleus counter, ranging in number density of 10^2 to 10^5 (particles per cm^3). A representation of the average size-distribution in typical atmospheric air is shown in Fig. 1 (Ref. 5). Two peaks below 3×10^{-6} cm are due to more aggregations of air and water molecules on ions, and are not foreign particles. Hence, the gas treated with physical filtration and electrical neutralization can be assumed to have such a size distribution of nuclei given by curves A, B or C.

In order to describe the number density and size distribution, a distribution function with respect to the droplet radius, R, should be defined. The distribution function N(R) multiplied by dR characterizes the number of particles lying in the size range from R to R + dR,

$$dN = N(R)dR \tag{1}$$

The overall particle concentration is then given by

$$< N > = \int_0^\infty N(R)dR \tag{2}$$

The assumed distribution functions in Fig. 1 can be expressed in a form of

$$\frac{dN}{d\ell nR} = N(R) \cdot R = N_o \left(\frac{R}{R_o}\right)^{2.5} \exp\left\{-\left(\frac{R}{R_o}\right)^{1.5}\right\} \tag{3}$$

where, N_o and R_o are given in Table 1, with other size average properties.

2.1.2 Shape and Size

Particles with a radius less than 10^{-6} cm (100 Å) are highly dispersed and in vigorous Brownian motion so that the shape of the particles is not at all spherical due to coagulation and sintering phenomena. It may, however, be possible to classify them by some effective particle size such as an average diameter or radius, although small pits, steps, cracks and cavities in the surface are the most important imperfections from a physical point of view of heterogeneous nucleation. Nevertheless, for simplicity, all particles are assumed to have a smooth, spherical shape of effective radius R, with a distribution function given by Eq. 3, without any further coagulation or separation.

2.1.3 Surface Physics and Chemistry

The main sources of Aitken nuclei are smoke and vapour from fires and industries, dust from the lands, salts from the oceans and particulate products from chemical reactions. The chemical and physical properties of these nuclei are extremely varied. This arises because the formation of the nuclei is due not only to a number of their originating processes but also to subsequent coalescence of particles, adsorption of gases, and chemical reactions. Hence, one may actually have reference only to average properties of particles.

If the nucleus consists of a mixture of soluble and insoluble particles, then nucleation is dominated by the soluble particles due to their smaller activation energy. The gases treated with physical and chemical processes can, however, contain a negligible quantity of soluble particles. Here, all condensation nuclei are assumed to be chemically inert and insoluble in water vapour.

2.2 Heterogeneous Nucleation

From the macroscopic point of view, heterogeneous nucleation follows steps very similar to homogeneous nucleation, although the former occurs on a surface immersed in a supersaturated vapour. Several models have been proposed for heterogeneous nucleation (Refs. 6, 7). According to these models, nucleation takes place as a result of growth beyond a critical size of embryos from a thermodynamic equilibrium distribution colliding with monomers or higher-order clusters. In addition, embryos can also form from adsorbed monomers or higher-order clusters in one or more layers on the solid surface.

The nucleation rate per unit surface area of particle per unit time can be basically expressed as,

$$\dot{n} = Z \cdot w \cdot n(i^*) \qquad (4)$$

where, $n(i^*)$ is the concentration of embryo of size i^*, on the substrate; w, the impingement rate of monomers on the embryo; and Z, the nonequilibrium correction factor.

2.2.1 Nucleation Mechanisms

Consider monomers or higher-order clusters of a supersaturated vapour impinging on a surface of a solid particle (R), to make a cap-shaped embryo (r),

as illustrated in Fig. 2. For heterogeneous nucleation, there are two types of monomer impingements on embryos; the direct impingement of monomers from the vapour and the impingement by desorption of adsorbed monomers.

(i) Direct impingement of monomers from vapour (Ref. 7)

According to kinetic theory, for a Maxwellian velocity distribution, the monomer flux J(1) is given by,

$$J(1) = \frac{p_v}{\sqrt{2\pi mkT}} \tag{5}$$

where, p_v is the vapour pressure, T the temperature, m the mass of one molecule and k the Boltzmann constant. The impingement rate of monomers on the embryo is then,

$$w = J(1)a_v^* \tag{6}$$

where, a_v^* is the surface area of the embryo.

The concentration of embryos of the size i* (number of monomers i*) can be approximately given by,

$$n(i^*) = n_s(1) \exp\left\{ - \frac{\Delta G^*(i)}{kT} \right\} \tag{7}$$

where, $n_s(1)$ is the concentration of adsorbed monomers on the substrate and $\Delta G^*(i)$ is the Gibbs free energy of formation of an embryo of size i*, from the vapour phase monomer of concentration $n_s(1)$.

The concentration of monomers adsorbed on the substrate can usually be written in terms of the impinging vapour flux J(1) and the mean manomer stay time on the substrate τ as,

$$n_s(1) = \alpha_a J(1)\tau \tag{8}$$

where, α_a is the adsorption coefficient and τ is given by,

$$\tau = \left\{ \nu \exp\left(- \frac{\Delta G_d}{kT} \right) \right\}^{-1} \tag{9}$$

where, ΔG_d is the desorption free energy of monomers and ν is the vibrational frequency of the adsorbed atom.

The nucleation rate per unit surface area of a nucleus particle by direct impingement of monomers from the vapour is then,

$$\dot{n} = \frac{\alpha_a p_v}{\sqrt{2\pi mkT}} \frac{1}{\nu} \exp\left(\frac{\Delta G_d}{kT}\right) \cdot Z \frac{p_v}{\sqrt{2\pi mkT}} a_v^* \exp\left(-\frac{\Delta G^*}{kT}\right) \qquad (10)$$

(ii) Impingement of adsorbed monomers on the substrate (Refs. 7, 8)

The rate at which adsorbed monomers impinge upon embryos on the substrate is given by (Ref. 8),

$$w = \ell_\ell \, \ell_s \, J(1)\tau \, \nu \exp\left(-\frac{\Delta G_s}{kT}\right) \qquad (11)$$

where, ℓ_ℓ is the embryo periphery, ℓ_s the mean surface diffusion distance and ΔG_s the free energy of activation for surface diffusion.

By substituting Eqs. 5, 7, 8, 9 and 11 into Eq. 4, the nucleation rate can be written as,

$$\dot{n} = \frac{\alpha_a p_v}{\sqrt{2\pi mkT}} \frac{1}{\nu} \exp\left(\frac{\Delta G_d}{kT}\right) \cdot Z \frac{p_v}{\sqrt{2\pi mkT}} \ell_\ell \, \ell_s \exp\left(\frac{\Delta G_d - \Delta G_s - \Delta G^*}{kT}\right) \qquad (12)$$

Using the reasonable assumption that $\Delta G_s \ll \Delta G_d$ and $\ell_\ell \, \ell_s \approx a_v^*$, both nucleation rate equations can be expressed in the same form as,

$$\dot{n} = Z \, a_v^* \frac{\alpha_a}{\nu} \left(\frac{p_v}{\sqrt{2\pi mkT}}\right)^2 \exp\left(-\frac{\Delta G^* - n\Delta G_d}{kT}\right) \qquad (13)$$

where, $n = 1$ for the direct impingement of monomers from vapour and $n = 2$ for the impingement of desorbed monomers. Thus, the difference between nucleation mechanisms of direct and indirect impingements of monomers can be included in the desorption free energy from a macroscopic point of view ($n\Delta G_d \rightarrow \Delta G_d$). In this sense, the nucleation rate per unit area of substrate can be expressed as,

$$\dot{n} = Z \, a_v^* \frac{\alpha_a}{\nu} \left(\frac{p_v}{\sqrt{2\pi mkT}}\right)^2 \exp\left(-\frac{\Delta G^* - \Delta G_d}{kT}\right) \qquad (14)$$

(iii) Nonequilibrium correction factor

Because the critical nuclei are steadily being consumed to produce droplets, the actual concentration of embryos and critical nuclei are smaller than the equilibrium values. The factor which corrects this embryo depletion is given by,

$$Z = \left\{ -\frac{1}{2\pi kT} \left(\frac{\partial^2 \Delta G}{\partial i^2}\right)_{i=i^*} \right\}^{\frac{1}{2}} \simeq \left\{ \frac{\Delta G^*}{3\pi kT i^*} \right\}^{\frac{1}{2}} \qquad (15)$$

for a cap-shaped embryo (Ref. 7), although it is not ordinarily a significant quantity in the nucleation rate.

(iv) The critical free energy ΔG^*

For embryos of small size, the partition functions for monomers and clusters including the translational, vibrational, rotational and configurational contributions should be evaluated to describe the free energy of embryo formation. However, because of its simplicity and mathematical tractability, a macroscopic approach is often used. By this method, the free energy of embryo formation can be expressed as the sum of contributions from the formation of the solid-liquid interface, the liquid-vapour interface, and the bulk:

$$\Delta G = \Delta G_b \, v_\ell + \sigma_{\ell v} \, a_v + (\sigma_{s\ell} - \sigma_{sv}) a_s \tag{16}$$

where, ΔG_b is the free-energy difference per unit volume of liquid phase from vapour to liquid phase, σ_{ij}, the surface free energy of the interface between phases i and j, v_ℓ, the volume of liquid, a_v, the surface area of liquid-vapour interface, a_s, the surface area of liquid-substrate interface and subscripts v, ℓ and s refer to vapour, liquid and substrate, respectively. From geometrical consideration, v_ℓ, a_v and a_s are written as,

$$\begin{aligned} v_\ell &= \frac{4}{3} \pi r^2 \, a \left(\frac{r}{R}, \cos\theta \right) \\ a_v &= 4\pi r^2 \, b_v \left(\frac{r}{R}, \cos\theta \right) \\ a_s &= 4\pi r^2 \, b_s \left(\frac{r}{R}, \cos\theta \right) \end{aligned} \tag{17}$$

where, a, b_v and b_s are a function of r/R and the contact angle θ, given in Appendix A, and in Fig. 3.

By using the usual definition of the contact angle

$$\cos\theta = \frac{\sigma_{s\ell} - \sigma_{sv}}{\sigma_{\ell v}} = \frac{\sigma_{s\ell} - \sigma_{sv}}{\sigma} \qquad (\sigma = \sigma_{\ell v}) \tag{18}$$

and substituting Eqs. 17 and 18 into Eq. 16, the free energy of formation of an embryo of radius r, on a nucleus of radius R, can be expressed as a function of r, R and $\cos\theta$. Differentiating ΔG with respect to r to evaluate the critical free energy ΔG^* gives the critical radius r^*,

$$r^* = - \frac{2\sigma}{\Delta G_b} \tag{19}$$

at which,

$$\left(\frac{\partial G}{\partial r} \right)_{r=r^*} = 0$$

The critical radius is identical with that for homogeneous nucleation. The free-energy difference between the vapour and liquid phases ΔG_b is,

$$\Delta G_b \doteq - n_\ell \, kT \, \ell n \left(\frac{p_v}{p_s} \right) = - n_\ell \, kT \, \ell n \, s \tag{20}$$

where, p_s is the saturation pressure of the vapour phase, n_ℓ, the number of molecules per unit volume of liquid and s, the supersaturation,

$$s = \frac{p_v}{p_s} \tag{21}$$

Substituting Eqs. 19 and 20 into Eq. 16 gives then the free energy of formation of a critical embryo (Ref. 9),

$$\Delta G^* = \frac{16\pi\sigma^3}{3(n_\ell \, kT \, \ell ns)^2} \, f\left(\frac{r^*}{R}, \cos\theta \right) \tag{22}$$

where,

$$f\left(\frac{r}{R}, \cos\theta \right) = \frac{1}{2}\left[1 + \left\{ c_\theta \left(\frac{r}{R} - \cos\theta \right) \right\}^3 + \left(\frac{R}{r} \right)^3 \left\{ 2 - 3c_\theta \left(1 - \frac{r}{R} \cos\theta \right) \right.\right.$$

$$\left.\left. + c_\theta^3 \left(1 - \frac{r}{R} \cos\theta \right)^3 \right\} + 3 \left(\frac{R}{r} \right)^2 \cos\theta \left\{ c_\theta \left(1 - \frac{r}{R} \cos\theta \right) - 1 \right\} \right] \tag{23}$$

$$c_\theta \equiv \left\{ 1 + \left(\frac{r}{R} \right)^2 - 2 \frac{r}{R} \cos\theta \right\}^{-\frac{1}{2}}$$

The factor $f(r/R, \cos\theta)$ is shown in Fig. 4. It means that lower values of contact angle reduce greatly the activation energy of the formation of critical embryo by virtue of the difference of surface free energy between vapour-solid and liquid-solid interfaces.

Finally, by combining Eqs. 14, 15 and 20, the heterogeneous nucleation rate per unit area of nucleus substrate can be expressed as,

$$\dot{n} = \dot{n}_o \, R_H \frac{b_s}{\sqrt{f}} \sqrt{\frac{T}{T_o}} \exp\left\{ \beta_d \left(\frac{T_o}{T} - 1 \right) \right\} \exp\left\{ - \frac{4\pi}{3} \frac{r^{*2}\sigma}{kT} (f - 1) \right\} \tag{24}$$

where, $\dot{n}_o$ means the homogeneous nucleation rate per unit volume of vapour,

$$\dot{n}_o \equiv 4\pi r^{*2} \frac{p_v}{\sqrt{2\pi mkT}} \frac{p_v}{kT} \exp\left(- \frac{4\pi}{3} \frac{r^{*2}\sigma}{kT} \right) \tag{25}$$

and

$$R_H = \frac{1}{v}\sqrt{\frac{kT_o}{2\pi m}}\, e^{\beta_d}, \qquad \beta_d = \frac{\Delta G_d}{kT_o}$$

2.2.2 Nucleation Rate

A nucleus particle has the surface area $A_o(= 4\pi R^2)$ at the initial stage of nucleation and the area comes to be wetted by condensed droplets, say A_s at time t. The surface area of a nucleus on which embryos can nucleate is,

$$A_e = A_o - A_s$$

Since the size distribution function of nuclei is N(R) and the nucleation rate per unit surface area of a nuclei is $\dot{n}$, the total nucleation rate per unit volume of vapour is then,

$$\dot{I} = \int_o^\infty \dot{n}\, A_e\, N(R)dR = \int_o^\infty \dot{n}(A_o - A_s)\, N(R)dR \tag{26}$$

The wetted surface area A_s is given by,

$$A_s = \int_o^t \dot{n}(\tau)\, (A_o - A_s)_\tau\, a_s(t,\tau)d\tau \tag{27}$$

where, $a_s(t,\tau)$ is the liquid-solid interfacial area of a condensed droplet which is formed at time τ ($< t$). The solution of the integral equation, Eq. 27, gives the wetted surface area of a nucleus A_s, hence the total nucleation rate $\dot{n}(A_o - A_s)$ or $\dot{I}$. The integral equation can be more easily solved by replacing it by successive differential equations (Appendix B), as follows:

$$\begin{aligned}
\frac{\partial A_s}{\partial t} &= \dot{n}(A_o - A_s)\, 4\pi r^{*2}\, b_s + \dot{r}_o\, B_s \\
\frac{\partial B_s}{\partial t} &= \dot{n}(A_o - A_s)\, 2\pi r^*\, c_{sb} + \dot{r}_o\, C_s \\
\frac{\partial C_s}{\partial t} &= \dot{n}(A_o - A_s)\, 2\pi\, c_{sc} + \dot{r}_o\, C_{s1} \\
\frac{\partial C_{s1}}{\partial t} &= \dot{n}(A_o - A_s)\, 2\pi\, c_{sc1} + \dot{r}_o\, C_{s2} \\
&\cdots
\end{aligned} \tag{28}$$

where, c_{sb}, c_{sc}, c_{sc1},... are a function of r/R and cosθ given by Eq. B-11 and $\dot{r}_o$ is the growth rate of homogeneously condensed nuclei given by Eq. 31 in the following.

2.3 Condensation and Droplet Growth

2.3.1 Droplet Growth

By using the Hertz-Knudsen equation for the net mass flow in unit time of vapour molecules condensing onto a droplet as in the homogeneous case (Ref. 1), the droplet growth rate can be approximately expressed as,

$$\frac{\partial}{\partial t}(\rho_\ell v_\ell) = a_v \frac{\alpha p_s}{\sqrt{2\pi mkT}} (s - 1) \tag{29}$$

where, $\rho_\ell v_\ell$ is the mass of a condensed droplet, a_v, its liquid-vapour surface area and α, the so-called condensation coefficient equal to the ratio of molecules sticking to the droplet to those impinging on it. The above relation with $\rho_\ell v_\ell = \rho_\ell 4\pi r^3 a/3$ yields

$$\dot{r} = \frac{b_v}{a}\left(1 + \frac{1}{3}\frac{r}{a}\frac{\partial a}{\partial r}\right)\dot{r}_o = K\dot{r}_o \tag{30}$$

where, $\dot{r}_o$ means the growth rate for homogeneous cases,

$$\dot{r}_o = \frac{\alpha}{\rho_\ell}\frac{p_s}{\sqrt{2\pi mkT}}(s - 1) \tag{31}$$

and

$$K = \frac{b_v}{a}\left(1 + \frac{1}{3}\frac{r}{a}\frac{\partial a}{\partial r}\right) \tag{32}$$

2.3.2 Condensate Mass

The mass of embryos produced during the time τ and $\tau + d\tau$ is,

$$\int_o^\infty \dot{n}(A_o - A_s)\rho_\ell v_\ell^* N(R)dRd\tau$$

which, grows at time t up to,

$$\int_o^\infty \dot{n}_\tau (A_o - A_s)_\tau \rho_\ell v_\ell(t,\tau)N(R)dRd\tau.$$

Thus, the overall condensate mass per unit mass of vapour mixture is given by,

$$g = \int_o^\infty g_R N(R)dR$$
$$g_R = \int_o^t \frac{\dot{n}_\tau}{\rho}(A_o - A_s)_\tau \rho_\ell v_\ell(t,\tau)d\tau \tag{33}$$

and the rate of production of the liquid phase by,

$$\frac{dg}{dt} = \int_o^\infty \frac{\partial g_R}{\partial t} N(R)dR \tag{34}$$

$$\frac{\partial g_R}{\partial t} = \left\{ \frac{\dot{n}}{\rho} (A_o - A_s)\rho_\ell v_\ell^* \right\}_t + \int_o^t \left\{ \frac{\dot{n}}{\rho} (A_o - A_s) \frac{\partial}{\partial t} (\rho_\ell v_\ell) \right\}_\tau d\tau$$

Further, when homogeneous nucleation is taken into account simultaneously, the rate of liquid-phase production can be written as,

$$\frac{dg}{dt} = \frac{\dot{n}_o}{\rho} \frac{4}{3} \pi r_o^{*3} \rho_\ell + \int_o^t \frac{\dot{n}_o}{\rho} \frac{d}{dt} \left(\frac{4}{3} \pi r_o^3 \rho_\ell \right) d\tau$$

$$+ \int_o^\infty \left[\frac{\dot{n}}{\rho} (A_o - A_s) \frac{4}{3} \pi r^{*3} a^* \rho_\ell \right.$$

$$\left. + \int_o^t \frac{\dot{n}}{\rho} (A_o - A_s) \frac{\partial}{\partial t} \left(\frac{4}{3} \pi r^3 a \rho_\ell \right) d\tau \right] N(R)dR \tag{35}$$

The first and second terms of the right-hand side are the contribution from homogeneous nucleation.

When the heterogeneous nuclei are in the size range of one or two orders larger than that of the embryos ($R \sim 10^{-5}$ cm) and the values of contact angle are not too large ($\theta < 120°$), heterogeneous nucleation is always favoured compared with homogeneous nucleation because of its smaller activation energy. For the same saturation, the heterogeneous nucleation rate, $\dot{n}$, is of one or two orders larger than the homogeneous, $\dot{n}_o$ (see Fig. 10). Consequently, in the present analysis, only the heterogeneous condensation terms are considered in the rate equation, Eq. 34.

The rate equation can be numerically solved by transforming them to successive differential equations (Appendix B), as follows:

$$\frac{\partial g_R}{\partial t} = 4\pi \rho_\ell \left\{ \frac{\dot{n}}{\rho} (A_o - A_s) \frac{r^{*3}}{3} a + \dot{r}_o A \right\}$$

$$\frac{\partial A}{\partial t} = \frac{\dot{n}}{\rho} (A_o - A_s) r^{*2} b_v + \dot{r}_o B$$

$$\frac{\partial B}{\partial t} = \frac{\dot{n}}{\rho} (A_o - A_s) r^* c_b + \dot{r}_o C \tag{36}$$

$$\frac{\partial C}{\partial t} = \frac{\dot{n}}{\rho} (A_o - A_s) c_c + \dot{r}_o C_1$$

$$\frac{\partial C_1}{\partial t} = \frac{\dot{n}}{\rho} (A_o - A_s) c_{c_1} + \dot{r}_o C_2$$

.....

where, c_b, c_c, c_{c_1},... are a function of r/R and cosθ given by Eq. B-7.

Since coefficients a, b_v, c's in Eq. 36 and b_s, c_s's in Eq. 28 are a function of the radius of nuclei R, the total mass fraction of liquid phase g should be obtained by integrating g_R with respect to R, which is extremely time-consuming for numerical computation. Hence, it may be sufficient to consider an appropriate approximation for the integration of these rate equations, before applying them to the problem of condensation of water vapour in a shock tube.

For example, consider the system of water-vapour and air mixtures, which contain nuclei particles with size distributions shown in Fig. 1 and have the initial conditions shown in Table 2. The pressure of the system is assumed to change as

$$\frac{p}{p_o} = 0.425 + 0.525 \exp(-30t^2) \tag{37}$$

which is nearly similar to the curve at -5 cm from the diaphragm in Fig. 12a. By combining the equations of energy and state, Eqs. 53 and 41, the rate equations, Eqs. 28 and 36, can be integrated numerically.

In Fig. 6 is shown the variation of condensate mass fraction with respect to time corresponding to the size distributions of nuclei, A, B and C in Fig. 1. In order to examine the effect of size distribution of nuclei, the following physical properties were used in Eq. 24:

$$R_H < R^2 > = 1, \qquad \beta_d = 34$$

which means $\nu = (1 \sim 10)\cdot 10^{13}$/sec and $\Delta G_d = 20$ kcal/mol. Equations 28 and 36 were integrated up to C_s and C, respectively. It is seen that because of the smaller values of embryo size compared with the effective radius of nuclei $r^* \ll R$, the size distribution has little influence on the result. By virtue of this fact, coefficients in Eqs. 28 and 36, a, bv, bs, c's and c_s's can be sufficiently approximated with their values in the limit of $r/R \to 0$, which are given by Eqs. A-4 and B-12. The rate equations are then reduced to the following ordinary differential equations:

$$\frac{dg}{dt} = < R^2 > \frac{dg_R}{dt} \tag{38}$$

$$\frac{dg_R}{dt} = 4\pi \rho_\ell \left\{ \frac{\dot{n}}{\rho} (1 - \bar{A}_s) \frac{r^{*3}}{3} a_\infty + \dot{r}_o A \right\}$$

$$\frac{dA}{dt} = \frac{\dot{n}}{\rho} (1 - \bar{A}_s) r^{*2} b_{v\infty} + \dot{r}_o B$$

$$\frac{dB}{dt} = \frac{\dot{n}}{\rho} (1 - \bar{A}_s) r^* c_{b\infty} + \dot{r}_o C \tag{39}$$

$$\frac{dC}{dt} = \frac{\dot{n}}{\rho} (1 - \bar{A}_s) c_{c\infty}$$

$$\frac{d\bar{A}_s}{dt} = \dot{n}(1 - \bar{A}_s)\, 4\pi r^{*2}\, b_{s\infty} + \dot{r}_o\, \bar{B}_s$$

$$\frac{d\bar{B}_s}{dt} = \dot{n}(1 - \bar{A}_s)\, 2\pi r^{*}\, c_{sb\infty} + \dot{r}_o\, \bar{C}_s \qquad (40)$$

$$\frac{d\bar{C}_s}{dt} = \dot{n}(1 - \bar{A}_s)\, 2\pi\, c_{sc\infty}$$

where

$$a_\infty = (1 - \cos\theta)^2 \left(\frac{1}{2} + \frac{1}{4}\cos\theta \right)$$

$$b_{v\infty} = \frac{1}{2}(1 - \cos\theta) \qquad b_{s\infty} = \frac{1}{4}(1 - \cos^2\theta)$$

$$c_{b\infty} = \frac{2}{2 + \cos\theta} \qquad c_{c\infty} = K_\infty\, c_{b\infty}$$

$$c_{sb\infty} = (1 - \cos^2\theta) \qquad c_{sc\infty} = K_\infty\, c_{sb\infty}$$

$$K_\infty = \frac{1}{2}\left\{ (1 + \cos\theta)\left(\frac{1}{2} + \frac{1}{4}\cos\theta \right) \right\}^{-1}$$

and $f(r/R, \theta)$ involved in $\dot{n}$ is,

$$f_\infty = (1 - \cos\theta)^2 \left(\frac{1}{2} + \frac{1}{4}\cos\theta \right) = a_\infty$$

Figures 7 to 10 show the effects of the vibrational frequency adatoms (R_H), the desorption free energy of monomers (β_d), and the contact angle (θ), upon the variations of temperature, supersaturation, condensate mass fraction and nucleation rate of embryos associated with the change in pressure given by Eq. 37. For smaller values of contact angle, heterogeneous nucleation occurs faster at lower supersaturation (Figs. 8 and 10), so that the decrease in temperature is smaller due to rapid heat release of condensation (Fig. 7). Larger values of the factor $R_H < R^2 >$ mean larger values of the concentration of adsorbed monomers on the nuclei, or the total surface area of nuclei, and accelerate heterogeneous nucleation, resulting in a higher nucleation rate at a lower supersaturation. Larger values of the factor β_d also mean higher concentrations of adsorbed monomers on the substrate and an increase in the nucleation rate.

The values of $\nu(R_H)$ and $\Delta G_d(\beta_d)$ are somewhat uncertain and depend largely upon the nucleation situation, but fortunately they are not significant quantities as seen in these figures. The features of heterogeneous nucleation and condensation are dominated largely by the contact angle, θ.

3. CONDENSATION OF WATER VAPOUR ON HETEROGENEOUS NUCLEI

The approach to the problem of condensation of water vapour in a shock tube is the same as in Ref. 1. A mixture of water vapour and air, which contains solid particles acting as heterogeneous nuclei, is suddenly expanded by a rarefaction wave in a shock tube and cooled until the vapour becomes supersaturated. Heterogeneous and homogeneous nucleation and condensation processes start. The associated variations of pressure, temperature, supersaturation, condensate mass and other physical quantities can be obtained by solving the gasdynamic equations coupled with the nucleation rate equations obtained in the preceding chapter.

3.1 Numerical Model

A mixture of water vapour and air or an inert carrier gas is initially at rest in the high-pressure driver section of a shock tube. At time t = 0, the diaphragm separating the driver section from the low-pressure channel section of the shock tube is suddenly ruptured, and the mixture is expanded into the channel. When sufficient supersaturation occurs, embryos of water-droplets nucleate heterogeneously on the substrate of solid particles contained in the carrier gas and then grow to larger water drops by condensation of water vapour. Concerning the gasdynamic and thermodynamic features of this system, the following assumptions are also made:

(i) The effects of molecular transport leading to viscosity, heat conduction and diffusion are neglected.

(ii) Solid particles move at the same speed as the mixture regardless of water-vapour condensation on them.

(iii) The thermodynamic properties of the mixture are the weighted sums of the corresponding properties for the single system.

3.1.1 Thermodynamic Properties

Let ρ_α be the density of species α, and $\mu\alpha$, its molecular weight. Denote the subscripts v, ℓ, s and i as vapour, liquid phase of water, solid particle and inert carrier gas, respectively. The equation of state for a mixture of water vapour and carrier gas is,

$$p = \left(\frac{\rho_i}{\mu_i} + \frac{\rho_v}{\mu_v} \right) \mathcal{R}\, T \tag{41}$$

where $\mathcal{R}$ is the universal gas constant. The mixture density is written as,

$$\rho = \rho_i + \rho_v + \rho'_\ell + \rho'_s \tag{42}$$

where, ρ'_ℓ and ρ'_s are the masses of liquid phase of water and solid particle per unit volume of the mixture, respectively. By defining the initial specific humidity ω_o, the condensate mass fraction g and the mass fraction of solid particle g_s as,

$$\omega_o = \frac{\rho_v + \rho'_\ell}{\rho} \qquad g = \frac{\rho'_\ell}{\rho} \qquad g_s = \frac{\rho_s}{\rho} \tag{43}$$

the equation of state, Eq. 41, can be rewritten as,

$$p = \left(\frac{1 - \omega_o - g_s}{\mu_i} + \frac{\omega_o - g}{\mu_v} \right) \rho \mathcal{R} T \tag{44}$$

The specific enthalpy of the mixture is,

$$h = \frac{\rho_i}{\rho} h_i + \frac{\rho_v}{\rho} h_v + \frac{\rho'_\ell}{\rho} h_\ell + \frac{\rho'_s}{\rho} h_s \tag{45}$$

where, h_α is the specific enthalpy of α-phase. By using the first law of thermodynamics,

$$h_\ell = h_v - L + c_\ell (T_\ell - T) \simeq h_v - L$$

where, L is the latent heat of vapourization and by taking the water vapour and the carrier gas to be thermodynamically perfect gases, the specific enthalpy and the specific internal energy of the mixture can be expressed as,

$$\begin{aligned} h &= c_{p_o} T - gL \\ e &= c_{p_o} T - gL - \frac{p}{\rho} \end{aligned} \tag{46}$$

where

$$c_{p_o} = (1 - \omega_o - g_s) c_{p_i} + \omega_o c_{p_v} + g_s \frac{h_s}{T}$$

The frozen sound speed in an ideal gas mixture is defined as,

$$a_f^2 = \left(\frac{\partial p}{\partial \rho} \right)_g = - \left(\frac{\partial h}{\partial \rho} \right)_{p,g} \left\{ \left(\frac{\partial h}{\partial p} \right)_{\rho,g} - \frac{1}{\rho} \right\}^{-1} \tag{47}$$

Using Eq. 46, the sound speed is then expressed as,

$$a_f^2 = \frac{c_{p_o} \mathcal{R} \left(\frac{1}{\mu_o} - \frac{g}{\mu_v} \right)}{c_{p_o} - \mathcal{R} \left(\frac{1}{\mu_o} - \frac{g}{\mu_v} \right)} T \tag{48}$$

where,

$$\frac{1}{\mu_o} = \frac{1 - \omega_o - g_s}{\mu_i} + \frac{\omega_o}{\mu_v}$$

The supersaturation s defined as the ratio of the pressure of the vapour phase to the saturation pressure is given by,

$$s = \frac{p_v}{p_s} = \frac{p}{p_s} \frac{\omega_o - g}{\frac{\mu_v}{\mu_o} - g} \tag{49}$$

where, p_s for water vapour is (Ref. 1),

$$p_s = 10^{(B-A/T)} \qquad A = 2263.0°K \qquad B \approx 6.064 \tag{50}$$

3.1.2 Gasdynamic Equations

By neglecting the effects of molecular transports according to assumption (i), the equations of continuity, momentum and energy are expressed as follows:

$$\frac{\partial \rho}{\partial t} + \frac{\partial}{\partial x}(\rho u) = 0 \tag{51}$$

$$\frac{\partial u}{\partial t} + u \frac{\partial u}{\partial x} = - \frac{1}{\rho} \frac{\partial p}{\partial x} \tag{52}$$

$$\frac{de}{dt} + p \frac{d}{dt}\left(\frac{1}{\rho}\right) = 0 \tag{53}$$

where, u is the velocity of the mixture and

$$\frac{d}{dt} = \frac{\partial}{\partial t} + u \frac{\partial}{\partial x}$$

These differential equations coupled with the nucleation rate equations can be solved numerically using the method of characteristics. As stated in Ref. 1, however, this method is not valid for flows when the characteristics intersect to form shock waves. For handling such a problem, Lax method can be used by smoothing the discontinuity through the nature of its differencing scheme by implicitly introducing a viscosity into the equations of motion.

Lax's scheme requires all differential equations to be expressed in the Lagrangian form, in which the coordinates and state variables of a flow particle are a function of time t and a parameter ξ, which identifies the particle. By

taking the spatial coordinate at the time origin t = 0, as the parameter, the equation of continuity can be written as,

$$\frac{\rho(\xi,0)}{\rho(\xi,t)} = \frac{\partial}{\partial \xi} x(\xi,t) \tag{54}$$

where, $\rho(\xi,t)$ is the density of particle ξ at time t and $x(\xi,t)$ is the coordinate of its spatial position $[\xi = x(\xi,0)]$. Since the particle velocity is,

$$u = \frac{\partial}{\partial t} x(\xi,t) \tag{55}$$

Equation 54 can be rewritten as,

$$\frac{\partial}{\partial t} \left\{ \frac{\rho(\xi,0)}{\rho(\xi,t)} \right\} = \frac{\partial u}{\partial \xi} \tag{56}$$

Using Eqs. 54 to 56, the momentum (52) and energy (53) equations reduce to

$$\frac{\partial u}{\partial t} = - \frac{1}{\rho(\xi,0)} \frac{\partial p}{\partial \xi} \tag{57}$$

$$\frac{\partial e}{\partial t} + \frac{p}{\rho(\xi,0)} \frac{\partial u}{\partial \xi} = 0 \tag{58}$$

The last equation is further rewritten by using Eq. 57 as,

$$\frac{\partial}{\partial t} \left(e + \frac{1}{2} u^2 \right) = - \frac{1}{\rho(\xi,0)} \frac{\partial}{\partial x} (pu) \tag{58a}$$

Equations 56 to 58 together with the rate equations, Eqs. 38 to 40, and the thermodynamic equations, Eqs. 44 to 50, describe the nonequilibrium heterogeneous condensation of water vapour in one-dimensional nonstationary flows. They can be solved numerically using Lax method following the same technique used in Ref. 1.

3.1.3 Numerical Model

Following Ref. 1, nondimensional quantities are now introduced.

$$\bar{p} = \frac{p}{p_o}, \quad \bar{\rho} = \frac{\rho}{\rho_o}, \quad \bar{T} = \frac{T}{T_o}, \quad \bar{u} = \frac{u}{a_o}, \quad \bar{e} = \frac{e}{a_o^2}$$

$$\bar{t} = \frac{t}{t_r}, \quad \bar{y} = \frac{\rho(\bar{y},0)}{\rho_c} \frac{\xi}{\ell}, \quad \bar{r} = \frac{r}{r_r} \tag{59}$$

$$\bar{A} = \rho_\ell A, \quad \bar{B} = \rho_\ell r_r B, \quad \bar{C} = \rho_\ell r_r^2 C, \quad \langle \bar{R}^2 \rangle = \langle R^2 \rangle r_r$$

where, quantities with subscript o refer to the condition in the driver section, a_o is the speed of sound and

$$\ell = a_o t_r, \qquad r_r = \sigma_r \left(\rho_\ell \frac{\mathcal{R}}{\mu_v} T_o \right)^{-1}$$

The gasdynamic equations become:

$$\frac{\partial \bar{v}}{\partial \bar{t}} = \frac{\partial \bar{u}}{\partial \bar{y}} \tag{60}$$

$$\frac{\partial \bar{u}}{\partial t} = - \frac{\partial}{\partial \bar{y}} \left(\frac{\bar{p}}{\gamma_o} \right) \tag{61}$$

$$\frac{\partial \bar{E}}{\partial \bar{t}} = - \frac{\partial}{\partial \bar{y}} \left(\frac{\bar{p}\,\bar{u}}{\gamma_o} \right) \tag{62}$$

where

$$\bar{v} = \frac{1}{\bar{\rho}}, \qquad \bar{E} = \bar{e} + \frac{1}{2} \bar{u}^2, \qquad \gamma_o = a_o^2 \frac{\rho_o}{p_o}$$

The thermodynamic equations are,

$$\bar{p} = \bar{\rho} \left(\frac{\mu_v}{\mu_o} - g \right) \frac{\mu_o}{\mu_v} \bar{T} \tag{63}$$

$$\bar{E} - \frac{1}{2} u^2 = \left\{ 1 + (\gamma_o - 1) \frac{\mu_o}{\mu_v} g \right\} \frac{\bar{T}}{\gamma_o (\gamma_o - 1)} - \frac{\lambda}{\gamma_o - 1} g \tag{64}$$

$$\bar{p}_v = \bar{\rho} (\omega_o - g) \frac{\mu_o}{\mu_v} \bar{T} \tag{65}$$

$$\bar{p}_s = \frac{\omega_o \mu_o}{\varphi_o \mu_v} 10^{A_1 (1 - 1/\bar{T})} \qquad A_1 = 2263.0/T_o \tag{66}$$

$$s = \frac{\bar{p}_s}{\bar{p}_v} \tag{67}$$

where

$$\lambda = \frac{L}{c_{p_o} T_o}, \qquad \varphi_o = \frac{p_{v_o}}{p_{s_o}} \; (= S_o)$$

The rate equations can be written as,

$$\frac{\partial \bar{g}}{\partial \bar{t}} = \langle \bar{R}^2 \rangle \frac{\partial \bar{g}_R}{\partial \bar{t}} \tag{68}$$

$$\left.\begin{aligned}
\frac{\partial \bar{g}_R}{\partial \bar{t}} &= 4\pi\,\theta \left\{ \frac{\dot{\bar{n}}}{\bar{\rho}} (1 - \bar{A}_s) \frac{\bar{r}^{*3}}{3} a_\infty + \dot{\bar{r}}\, \bar{A} \right\} \\
\frac{\partial \bar{A}}{\partial \bar{t}} &= \frac{\dot{\bar{n}}}{\bar{\rho}} (1 - \bar{A}_s)\, \bar{r}^{*2}\, b_{v\infty} + \dot{\bar{r}}_o\, \bar{B} \\
\frac{\partial \bar{B}}{\partial \bar{t}} &= \frac{\dot{\bar{n}}}{\bar{\rho}} (1 - \bar{A}_s)\, \bar{r}^{*}\, c_{b\infty} + \dot{\bar{r}}_o\, \bar{C} \\
\frac{\partial \bar{C}}{\partial \bar{t}} &= \frac{\dot{\bar{n}}}{\bar{\rho}} (1 - \bar{A}_s)\, c_{c\infty}
\end{aligned}\right\} \tag{69}$$

$$\left.\begin{aligned}
\frac{\partial \bar{A}_s}{\partial \bar{t}} &= \theta_s \{ \dot{\bar{n}} (1 - \bar{A}_s)\, 4\pi \bar{r}^{*2}\, b_{s\infty} + \dot{\bar{r}}_o\, \bar{B}_s \} \\
\frac{\partial \bar{B}_s}{\partial \bar{t}} &= \dot{\bar{n}} (1 - \bar{A}_s)\, 2\pi \bar{r}^{*}\, c_{sb\infty} + \dot{\bar{r}}_o\, \bar{C}_s \\
\frac{\partial \bar{C}_s}{\partial \bar{t}} &= \dot{\bar{n}} (1 - \bar{A}_s)\, 2\pi\, c_{sc\infty}
\end{aligned}\right\} \tag{70}$$

where

$$\dot{\bar{n}} = \dot{n}_o \frac{R_h}{r_r} \frac{b_{s\infty}}{\sqrt{f}} \sqrt{\bar{T}} \exp\left\{ \beta_d \left(\frac{1}{\bar{T}} - 1 \right) \right\} \exp\left\{ - \frac{\bar{W}\, \bar{\sigma}^3}{\bar{T}^3\, \ell n^2\, \bar{s}} (f - 1) \right\} \tag{71}$$

$$\dot{\bar{n}}_o = \frac{\mu_v}{\mu_o}\sqrt{\bar{\sigma}}\,\frac{\bar{p}}{\bar{T}}\,\frac{(\omega_o - g)^2}{\left(\frac{\mu_v}{\mu_o} - g\right)}\exp\left(-\frac{\bar{W}\,\bar{\sigma}^3}{\bar{T}^3\,\ell n^2\bar{s}}\right) \qquad \bar{W} \equiv \frac{16\pi r_r^2\sigma_r}{3kT_o} \tag{72}$$

$$\dot{\bar{r}} = G_r\,\frac{\alpha\,\bar{p}_s}{\sqrt{2\pi\bar{T}}}\,(\bar{s} - 1) \qquad G_r \equiv \frac{p_o}{\sigma_r}\sqrt{\frac{\mathcal{R}T_o}{\mu_v}}\,t_r \tag{73}$$

$$\bar{r}^* = \frac{2\bar{\sigma}}{\bar{T}\,\ell n\,\bar{s}} \tag{74}$$

$$\Theta \equiv \rho_\ell\, r_r^3\, G_n\, t_r \qquad \Theta_s \equiv \rho_o\, r_r^2\, G_n\, t_r$$

$$r_r \equiv \sigma_r\left(\rho_\ell\,\frac{\mathcal{R}}{\mu_v}\,T_o\right)^{-1} \qquad G_n \equiv \frac{\dot{n}_o}{\rho_o\,\dot{\bar{n}}_o} = \sqrt{\frac{2\sigma_r}{\pi}}\left(\frac{N_A}{\mu_v}\right)^{3/2}\frac{\rho_o}{\rho_\ell}$$

The surface tension is assumed to vary linearly with temperature in the same way as used in Ref. 1,

$$\bar{\sigma} = \frac{\sigma}{\sigma_r} \approx 1.693 - 0.00254T_\circ\,\bar{T} \qquad \sigma_r \equiv 75.6\ \text{dyne/cm}^2 \tag{75}$$

The latent heat of condensation is taken as L = 623 cal/g. Other physical quantities are the same as those used in Ref. 1, and given in Tables 1 and 2 of the paper. Concerning the physical properties of solid particles, those of S_iO_2 are used, although they have negligible effect on the overall properties of the mixture.

Detailed data on contact angles in the system of solid particles of Aitken nuclei wetted by water are not available. The angles $\theta = 60°$, 90° and 120° are taken as representative values. Although the values of the vibrational frequency of adsorbed atoms and the free energy of desorption are not certain, they are roughly estimated as $\nu = (0.1 \sim 10)\ 10^{13}$/sec and $\Delta G_d = (2 \sim 200)\ 10^3$ cal/g-atom (Ref. 8), that is,

$$R_H = 10^4 \sim 10^8\ \text{cm}, \qquad \beta_d = \frac{\Delta G_d}{kT_o} = 3 \sim 300$$

Equations 60 to 74, with the foregoing physical properties, were solved numerically for the same case used in Ref. 1 by employing the same Lax computational technique. However, in the present calculations, the mesh sizes of space and time coordinates were changed. The size of space mesh chosen, $\Delta y = 1/400$, which corresponds to a distance of about 1 mm between two particle paths (cf. 0.5 mm in Ref. 1). Doubling the size of space mesh is associated with the

truncation error of about 5 ~ 10% compared with the results of 1/800 mesh size, but it decreases the computational time by a factor of about three or four. The stability condition time-increment constant,

$$\xi_c = \frac{\Delta\bar{t}}{\Delta\bar{y}} (\bar{\rho}\ \bar{a}_f)_{max}$$

was selected as $\xi_c = 0.25$ (cf. 0.75 in Ref. 1) in order to diminish the error associated with the increased space-mesh size. A Lax dissipation factor, $\mu = 0.2$, was used. The numerical computations were performed on an IBM 370-165 at the Institute of Computer Science, University of Toronto.

3.2 Numerical Results and Discussions

3.2.1 Comparison with Homogeneous Nucleation

Figures 11 to 15 show the results of the present numerical calculations of heterogeneous condensation of water vapour in a shock tube. They are compared with those of homogeneous condensation. The numerical constants of heterogeneous nucleation are

$$< R^2 > = 3.12 \times 10^{-6}\ cm^2\ cm^{-3} \text{ (Curve B in Fig. 1)}$$

$$\theta = 90°, \qquad R_H = < R^2 >^{-1} = 0.311 \times 10^6\ cm, \qquad \beta_d = 34$$

Although the effects of these constants will be discussed in detail in the next section, the obtained results are considerably influenced by the value of the contact angle.

The predicted flow field of the nonequilibrium nonstationary rarefaction wave in the physical $(\bar{x}, \bar{t})$-plane is shown in Fig. 11. The head of the rarefaction wave moves into the mixture at rest with the state sound speed. Behind the rarefaction, the mixture is cooled to supersaturation. Consequently, nucleation takes place on the heterogeneous nuclei with an appropriate time lag. In the figure, the condensation wave is defined as the locus of points along particle paths where the supersaturation reaches its maximum values (cf. Fig. 14b). Owing to the heat release associated with condensation, the condensation wave is followed by a shock wave, which is strictly defined by the locus of intersection points of left-running characteristics (see Ref. 1). In the present representation, however, the shock wave is defined by the locus of points of the pressure maximum after supercooling. Between the condensation wave front and the shock wave, there exists a condensation zone, hatched in the figure, where the flow variables change appreciably due to heat release. It can be seen from the figure that condensation in the heterogeneous case ($\theta = 90°$) occurs sooner than in the homogeneous case (HM). The width between two fronts is also narrower for $\theta = 90°$. The frozen isentropic tail of the wave corresponds to a frozen Mach number for a diaphragm pressure ratio ($M_{f_o} = 0.784$).

Figures 12 to 15 show time and space variations of the pressure, temperature, supersaturation and condensate mass fraction, a) along three particle

paths, initially at -5 (a), -10 (b) and -20 (c) cm from the diaphragm of the shock tube, and b) at four time levels, 0.48 (a), 0.72 (b), 0.96 (c) and 1.2 (d) msec. As shown in Figs. 12 to 13, in heterogeneous condensation, the decrease in the pressure and temperature before the onset of condensation is smaller than that in homogeneous condensation. The successive rise of their values after the onset of condensation is also smaller. The onset of condensation occurs for particle paths farther from the diaphragm or at lower time levels. Space and time variations of supersaturation are shown in Fig. 14. It is readily seen that heterogeneous nucleation leads to lower values of maximum supersaturation since the onset of condensation occurs closer to the wave head. Variations of the condensate mass fraction are plotted in Fig. 15. In the heterogeneous cases, the condensate mass fraction increases more sharply up to the equilibrium value.

Since the supersaturation is directly related to the nucleation rate, the latter attains its maximum approximately at the highest supersaturation. Thereafter, the condensation of water vapour onto the solid nuclei plays an increasingly important role in the phase-changing process. The increased heat release due to condensation causes an increase in the temperature of the mixture. In heterogeneous nucleation, the activation energy is greatly reduced by the fact that the interfacial free energy of the chemical bond between vapour atoms and substrate is larger than that between liquid atoms and substrate ($\sigma_{sv} > \sigma_{s\ell}$) and their difference reduces the overall interfacial energy for formation of the liquid-vapour interface of embryos. This acts equivalently to decrease the surface tension. Less activation energy results in a higher nucleation rate with lower supersaturation, lower supercooling, a higher propagation velocity of the condensation wave, and a narrower condensation zone.

3.2.2 Effects of Physical Properties of Nuclei

It is shown in Chapter 2 that the size distribution of condensation nuclei hardly affects the condensation process in the expansion of the mixture, unless their size is comparable to that of nucleating embryos. For such a size distribution as that of Aitken nuclei shown in Fig. 1, the property which contributes directly to the nucleation process is the total surface area of the nucleus $< R^2 >$. Other factors controlling the heterogeneous nucleation are the concentration of adsorbed monomers on the surface of the substrate and the contact angle of embryo. The former is characterized by the vibrational frequency of adatoms $\nu(R_H)$ and the desorption free energy of adsorbed monomers $\Delta G_d(\beta_d)$. Since the activation energy of nucleation is much larger than the desorption energy of adsorbed monomers, the latter does not greatly affect the nucleation process but reduces slightly the overall activation energy of nucleation. Thus, the factor R_H has a physical meaning related to the concentration of monomers adsorbed onto the surface of the substrate. It is a constant coefficient of the nucleation rate $\dot{n}$. For the sake of reducing computer costs, only the contact angle θ, and the factor R_H, were considered as the physical parameters that affect the flow field of the nonequilibrium nonstationary rarefaction wave of water-vapour/carrier-gas mixture in a shock tube. In the expression of the condensate mass, however, the factor R_H is always coupled with the overall surface area $< R^2 >$. The influence of the overall surface area or the overall number of nuclei can be inferred by inspection of the effect of the factor R_H.

Figures 16 to 21 show the effects of the contact angle θ and the factor R_H. For cases to compare the effects of the contact angle, $R_H = 0.311 \times 10^6$ cm

is used. For the curves denoted by R_H', $R_H = 0.311 \times 10^4$ cm and $\theta = 90°$ are used. The flow fields in the $(\bar{x}, \bar{t})$ plane are shown in Figs. 16 and 17, the effects of the contact angle ($\theta = 90°$, 120°) and the factor R_H ($R_H \approx 10^6$, 10^4 cm), respectively. For larger contact angles, which means embryos of more spherical shape, the heterogeneous nucleation loses its influence and tends to have the features of homogeneous nucleation. Reducing the value of the factor R_H leads to a lower nucleation rate and higher supercooling. Figures 18 to 21 are the time and space variations of the pressure, temperature, supersaturation and condensate mass fraction, respectively. In the curves denoted by R_H', the factor R_H is of two orders less than that of other curves. It does, however, have an influence less than that of $\theta = 120°$. It is the contact angle that really characterizes the significant feature of heterogeneous condensation. It should be noted that, for an accurate prediction of the flow field of heterogeneous condensation, the contact angle of embryos nucleating on the substrate of solid particles must be carefully estimated. Yet, other parameters, including the overall surface area of the nuclei can be roughly estimated without serious effects. Nevertheless, there is no precise knowledge to make reasonably good choices possible until existing experimental data from various experiments are correlated.

3.2.3 Comparison with Experimental Data

The numerical results can be compared with Kalra's experimental study of a nonstationary expansion of water-vapour-nitrogen mixture in a shock tube (Ref. 10). Following the same considerations of the pressure history discussed in Ref. 1, the space location of the experimental measurement, $x = -17.0$ cm from the diaphragm, is selected as corresponding to $x = -23.4$ cm. To obtain a reasonable fit with the experimental data in Ref. 1, the surface tension was changed from the value of the semi-empirical expression, Eq. 75, $\sigma = 82$ dynes/cm to 68 dynes/cm, with the conclusion that choosing a suitable value for the surface tension provides a good fit for the experiments. As shown in Fig. 22, in heterogeneous condensation, a similar fit can be obtained by replacing the surface tension by the contact angle. By choosing a suitable value for the contact angle ($\theta \approx 90°$), the experimental data can be fitted fairly well except for the supersaturation at the onset of condensation, which is shown in brackets in Fig. 22.

Figure 23 is a comparison with the experimental data as plotted for the empirical relation between the supercooling and the cooling rate derived by Kalra (Ref. 10):

$$\frac{T_s - T_c}{T_c} = 0.85 \times 10^{-3} \left(- \frac{dT}{dt} \right)^{0.46}$$

where, T_s is the temperature of equilibrium saturation, T_c the temperature at the onset of condensation, and $(-dT/dt)$ the rate of cooling. Concerning this relation, the discrepancies with the numerical results are quite appreciable. The best-fit conditions of the pressure history in Fig. 22, $\theta = 90°$, in the heterogeneous case, and $\sigma = 68.0$ dynes/cm, in the homogeneous case, result in the poorest agreement in Fig. 23. Owing to the limited experimental data, it is not certain whether this is due to the inadequacies of the models or features of the experimental data, such as the estimation of temperature from the pressure profiles, for example, or whether the waves are planar. It cannot be concluded at present which process, heterogeneous or homogeneous condensation, adequately explains the experimental data.

It should also be noted that the best fits for homogeneous and heterogeneous nucleation and condensation will give points very close to each other on the time-distance plot shown in Sislian's Fig. 49 (Ref. 1). Consequently, the schlieren records of Glass and Patterson (Ref. 11) cannot be used as a decisive test for the two competing theories, since the trajectory of the condensation shock agrees with either point (only) from the two theories.

An inspection of Fig. 22 shows that the experimental time-variation of pressure at the onset of condensation is extremely sharp compared with the numerical results. This is not surprising in view of the fact that the implicit artificial viscosity used in the numerical analysis tends to spread the condensation and shock fronts. It is also worth noting that factors such as coagulation, solubility, or electrical charges have not been treated in this analysis. Physical data in these areas are lacking.

4. CONCLUDING REMARKS

By using a macroscopic model of heterogeneous nucleation, a theoretical study was made of the condensation of water-vapour/carrier-gas mixtures in a nonequilibrium nonstationary rarefaction wave generated in a shock tube. The present analysis is compared with the results of homogeneous nucleation. Nucleation is assumed to take place heterogeneously on idealized smooth, spherical solid particles of Aitken nuclei, which are chemically and electrically inert.

In the process of heterogeneous nucleation, the controlling factors are the size distribution of nuclei, the concentration of monomers adsorbed on the surface of the substrate and the contact angle of embryos. Of these factors, the dominant one is the contact angle. By decreasing the contact angle, the activation energy of nucleation is greatly reduced due to the fact that the formation of a liquid-vapour interface is replaced by a liquid-solid interface having a lower interfacial free energy. At less supercooled states and lower supersaturations, the onset of condensation occurs closer to the wave head where temperatures and pressures are higher. The reverse is true for homogeneous condensation.

When nuclei are in the size range of one or two orders larger than that of the embryos ($R \sim 10^{-5}$ cm) and the value of the contact angle is not too large ($\theta < 120°$), heterogeneous nucleation dominates the condensation process and homogeneous nucleation can be neglected. In this case, the size distribution of nuclei affects the overall nucleation and condensation only through the total surface area of the nuclei. The concentration of monomers adsorbed on the surface of the substrate is dominated by the vibrational frequency and the desorption energy of adatoms. These act as a factor on which the nucleation rate has a linear dependence. The reduction in the total surface area of nuclei and the factor depending on the surface concentration of monomers results in weakening the effect of the contact angle.

The nucleation rate is very sensitive to the contact angle. Consequently, its value should be carefully chosen. An appropriate value for the contact angle makes it possible to fit the numerical results with experimental data. From the data available at UTIAS, a contact angle of 90° appears reasonable. However, this does not substitute for an actual measurement. Perhaps it is only indicative of an averaged result, $\bar{\theta} = 90°$. This is such an important quantity for heterogeneous nucleation that it makes an experimental determination imperative.

In the present theory, the shape of embryo and substrate different from a sphere, the electric charge and the solubility of nuclei were not taken into account. These are important factors that can significantly reduce the activation energy, thereby increasing the heterogeneous nucleations. To examine the effects of such factors, the present theory can be readily extended. However, other uncertainties would be introduced when selecting suitable values for the corresponding physical properties.

When nuclei or embryos have a higher number density, coagulation owing to Brownian motion takes place and is another factor to be considered. By assuming the coagulation constant as 10^{-9} $cm^3/(sec\ particles)$ (Ref. 12) and the characteristic time as 10^{-3} sec, the number density above which coagulation has a considerable effect can be estimated as 10^{12} particles/cm^3. Since the assumed number density of heterogeneous nuclei is about 10^5 particles/cm^3, coagulation hardly affects the results within such a characteristic time. In the homogeneous nucleation case, however, it may be a factor to be taken into account because of the higher number density of nucleated droplets ($> 10^{15}$ particles/cm^3, see Ref. 1). Kalra's experimental results can be explained equally by both homogeneous and heterogeneous nucleation theories with suitable values of surface tension and contact angle, respectively. In view that the former requires a lower value of surface tension and a possible consideration of coagulation, heterogeneous nucleation and condensation would be closer to the experiments. However, the fact that the contact angles have not been measured throws some doubt on that analysis. It must therefore be concluded that the choice of model, heterogeneous or homogeneous condensation, can only be settled by a decisive set of experiments.

REFERENCES

1. Sislian, J. P. — Condensation of Water Vapour With or Without a Carrier Gas in a Shock Tube. UTIAS Report No. 201, 1975.

2. Turnbull, D. — Progress in Solid State Physics, Vol. 3, Academic Press, New York, 1956.

3. Walton, D. — Nucleation of Vapor Deposits. J. Chem. Physics, Vol. 37, p. 2182, 1962.

4. Fletcher, N. H. — The Physics of Rainclouds. Cambridge Univ. Press, Cambridge, 1962.

5. Junge, C. — Gesetzmässigkeiten in der Grössenverteilung Astmosphärischer Aerosole über den Kontinent. Ber. dtsch. Weterdienst (U.S. Zone), Vol. 35, p. 264, 1952.

6. Hirth, J. P.; Pound, G. M. — Condensation and Evaporation, Nucleation and Growth Kinetics. Pergamon Press, Oxford, 1963.

7. Sigsbee, R. A. — Vapor to Condensed-Phase Heterogeneous Nucleation. In Nucleation, ed. by A. C. Zettlemoyer, M. Dekker, New York, Ch. 4, 1969.

8. Pound, G. M.; Simnad, M. T.; Yang, L. — Heterogeneous Nucleation of Crystals from Vapor. J. Chem. Physics, Vol. 22, p. 1215, 1954.

9. Fletcher, N. H. — Size Effect in Heterogeneous Nucleation, J. Chem. Physics, Vol. 29, p. 572, 1958.

10. Kalra, S. P. — Experiments on Nonequilibrium, Nonstationary Expansion of Water Vapor/Carrier Gas Mixtures in a Shock Tube. UTIAS Report No. 195, 1975; also Private Communication.

11. Glass, I. I.; Patterson, G. N. — A Theoretical and Experimental Study of Shock Tube Flows. J. Aero. Sci., Vol. 22, p. 75, 1955.

12. Green, H. L.; Lane, W. R. — Particulate Clouds; Dusts, Smokes and Mists. E. & F. N. Spon Ltd., London, 1964.

TABLE 1

SIZE DISTRIBUTION FUNCTION OF NUCLEI

$$N(R) \cdot R = N_o \left(\frac{R}{R_o}\right)^{2.5} \exp\left\{-\left(\frac{R}{R_o}\right)^{1.5}\right\}$$

		A	B	C
N_o	cm^{-3}	1.0×10^{5}	1.0×10^{5}	1.0×10^{5}
R_o	cm	1.5×10^{-6}	2.5×10^{-6}	5.0×10^{-6}
Total number $< N >$	cm^{-3}	3.33×10^{4}	3.33×10^{4}	3.33×10^{4}
Total surface area $< R^2 >$	$cm^2 \cdot cm^{-3}$	1.12×10^{-6}	3.12×10^{-6}	1.25×10^{-5}
Total volume $< R^3 >$	$cm^3 \cdot cm^{-3}$	9.42×10^{-13}	4.36×10^{-12}	3.49×10^{-11}
Mean radius $< R > / < N >$	cm	1.36×10^{-6}	2.26×10^{-6}	4.51×10^{-6}
Mean surface area $< R^2 > / < N >$	cm^2	3.37×10^{-11}	9.35×10^{-11}	3.74×10^{-10}
Mean volume $< R^3 > / < N >$	cm^3	2.83×10^{-17}	1.31×10^{-16}	1.05×10^{-15}

$$< N > \equiv \int_0^\infty N(R)dR \qquad < R > \equiv \int_0^\infty R.N(R)dR$$

$$< R^2 > \equiv \int_0^\infty 4\pi R^2 \cdot N(R)dR \qquad < R^3 > \equiv \int_0^\infty \frac{4}{3}\pi R^3 \cdot N(R)dR$$

TABLE 2

INITIAL CONDITIONS IN THE SHOCK TUBE

Driver Conditions

Mixture of water vapour and nitrogen

ω_o = 0.0176

φ_o = 0.9727

p_{vo} = 18.6 mm Hg

p_{so} = 19.23 mm Hg

p_o = 680 mm Hg

ρ_o = 0.1025×10^{-2} g/cm^3

T_o = 295.3°K

a_o = 352.2 m/sec

Channel Conditions

Air

p_1 = 100 mm Hg

T_1 = 295.3°K

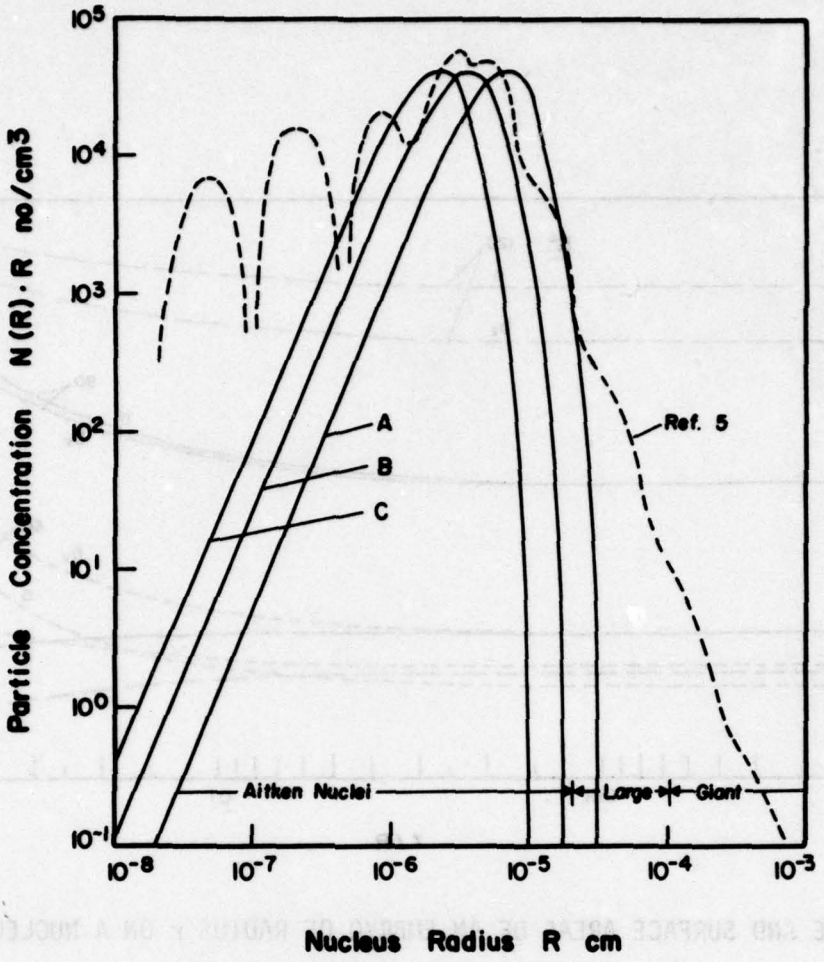

FIG. 1 SIZE DISTRIBUTION OF NUCLEUS PARTICLES

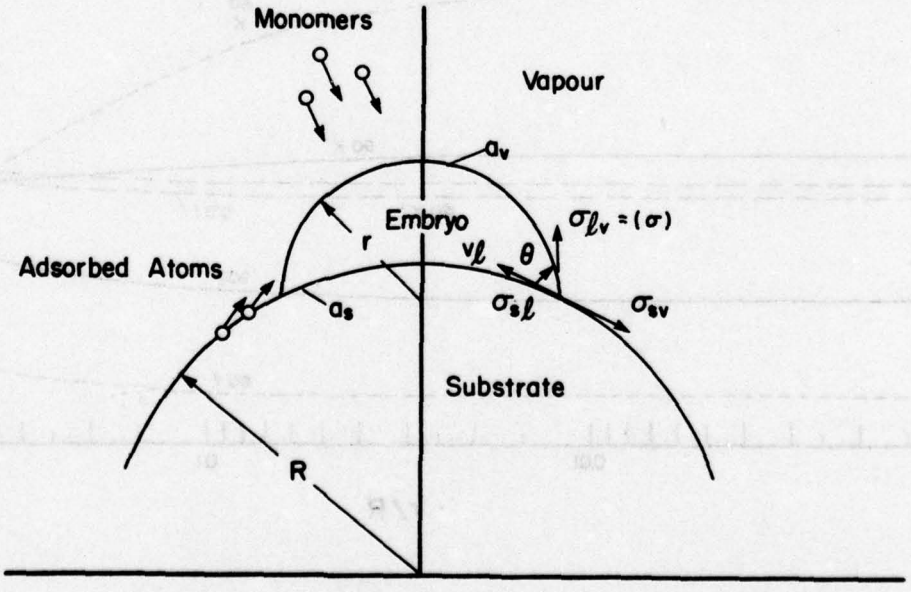

FIG. 2 CAP-SHAPED EMBRYO NUCLEATING ON SURFACE OF INSOLUBLE SUBSTRATE

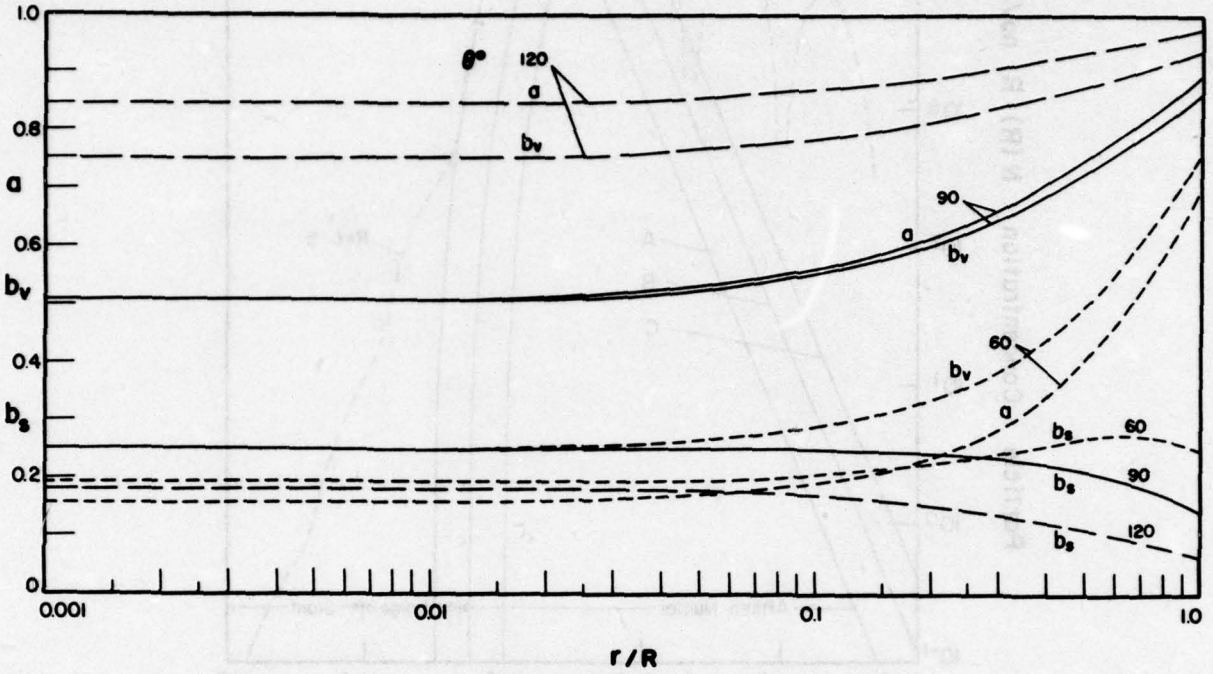

FIG. 3 VOLUME AND SURFACE AREAS OF AN EMBRYO OF RADIUS r ON A NUCLEUS OF RADIUS R

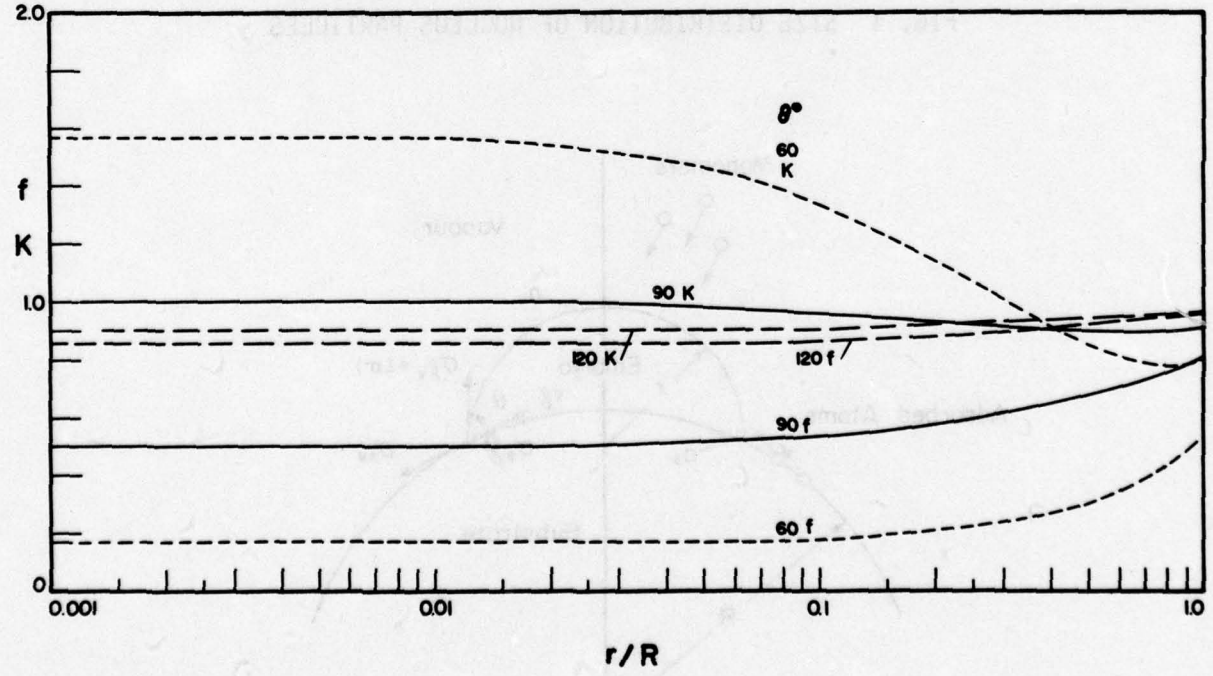

FIG. 4 COEFFICIENTS (f, K) IN NUCLEATION RATE EQUATIONS

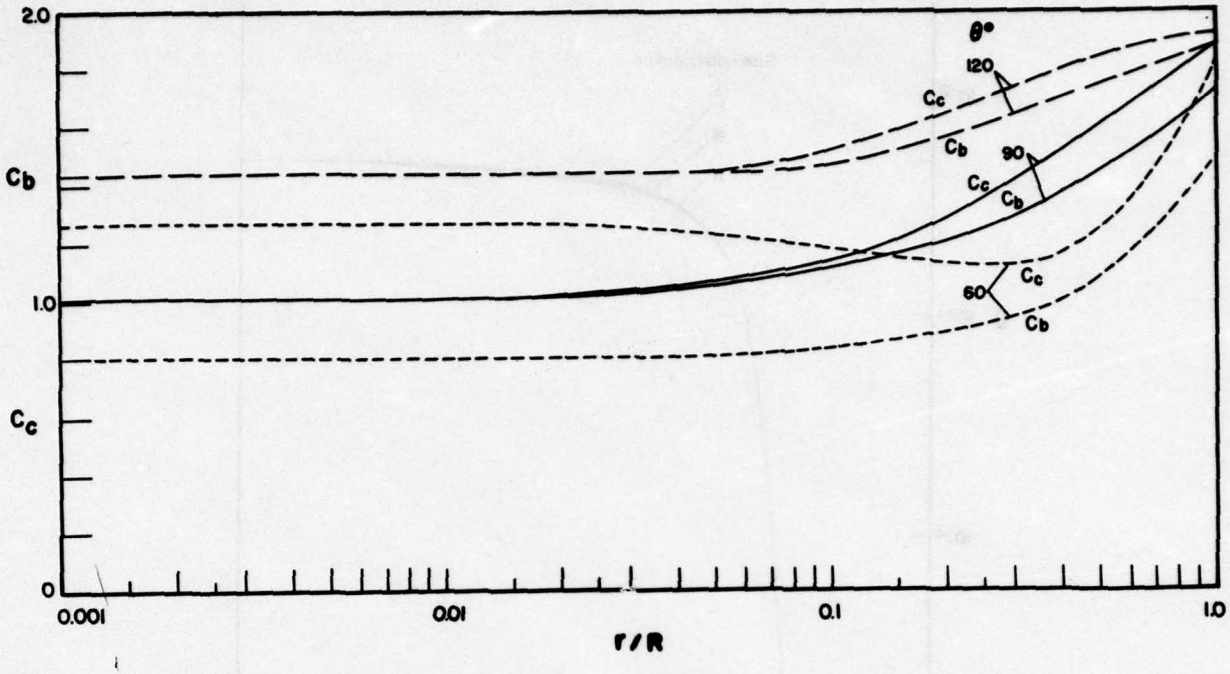

FIG. 5-a COEFFICIENTS (C_b, C_c) IN NUCLEATION RATE EQUATIONS

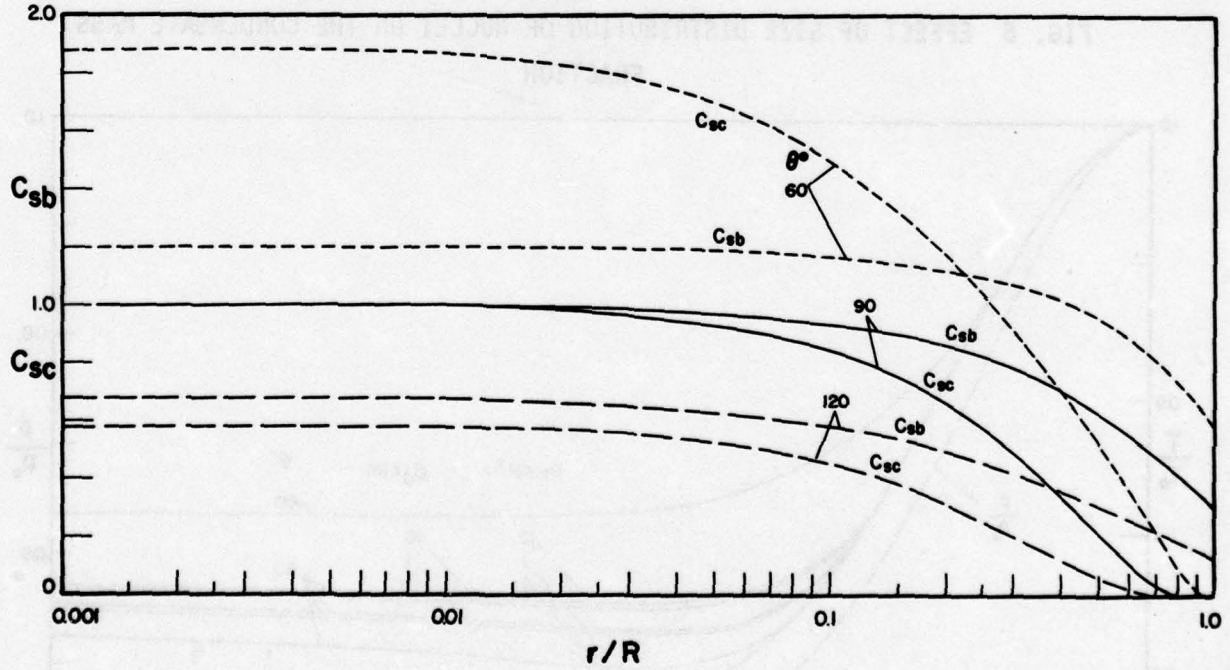

FIG. 5-b COEFFICIENTS (C_{sb}, C_{sc}) IN NUCLEATION RATE EQUATIONS

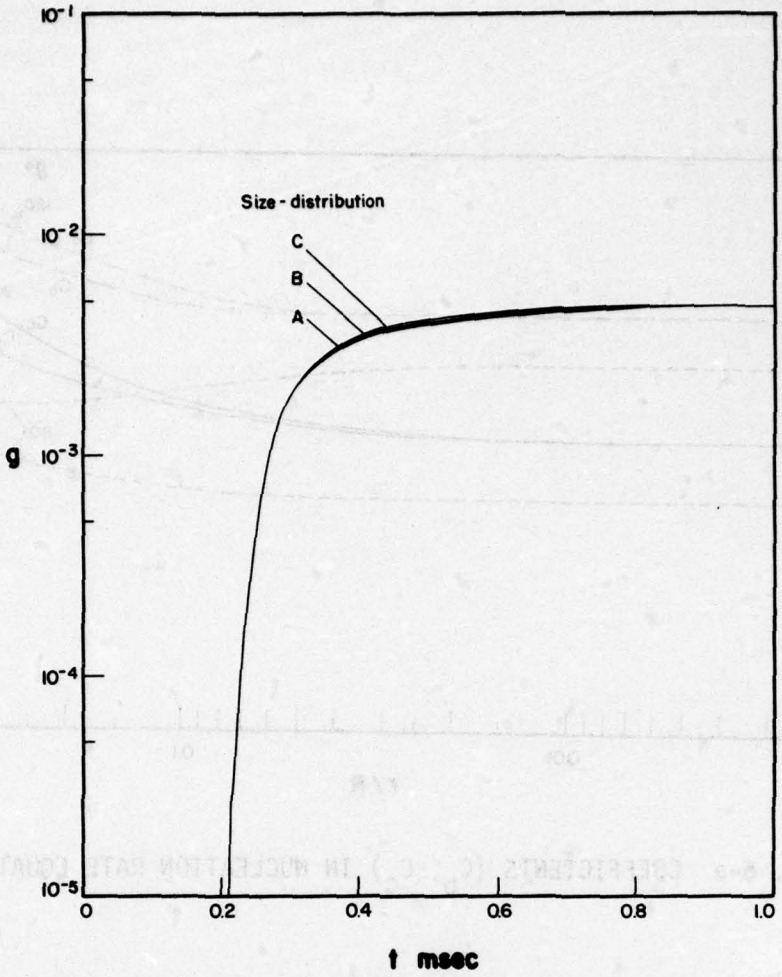

FIG. 6 EFFECT OF SIZE DISTRIBUTION OF NUCLEI ON THE CONDENSATE MASS FRACTION

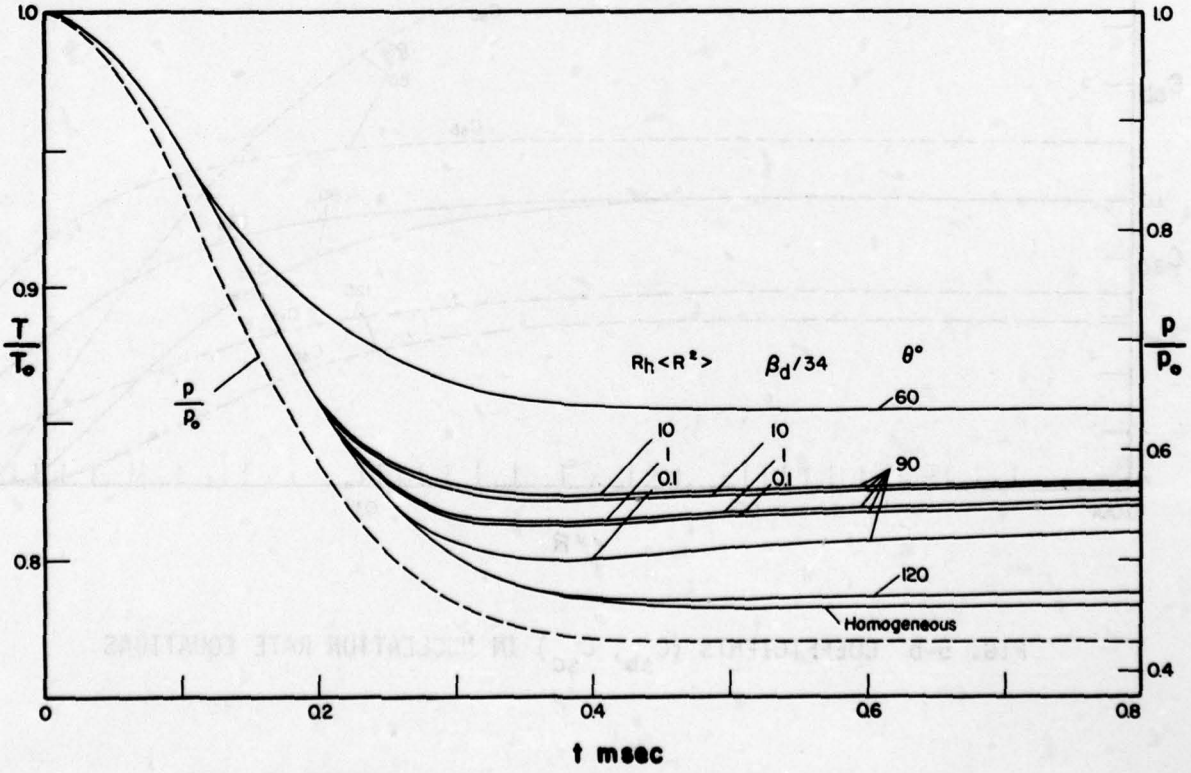

FIG. 7 EFFECT OF PHYSICAL PROPERTIES ON TEMPERATURE

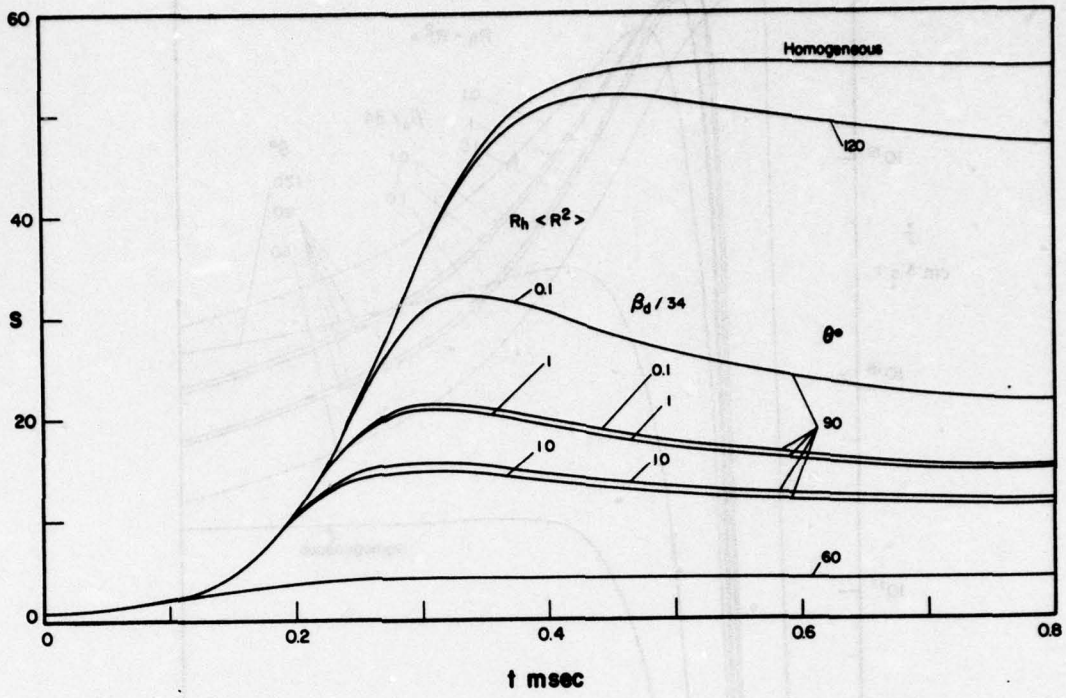

FIG. 8 EFFECT OF PHYSICAL PROPERTIES ON SUPERSATURATION

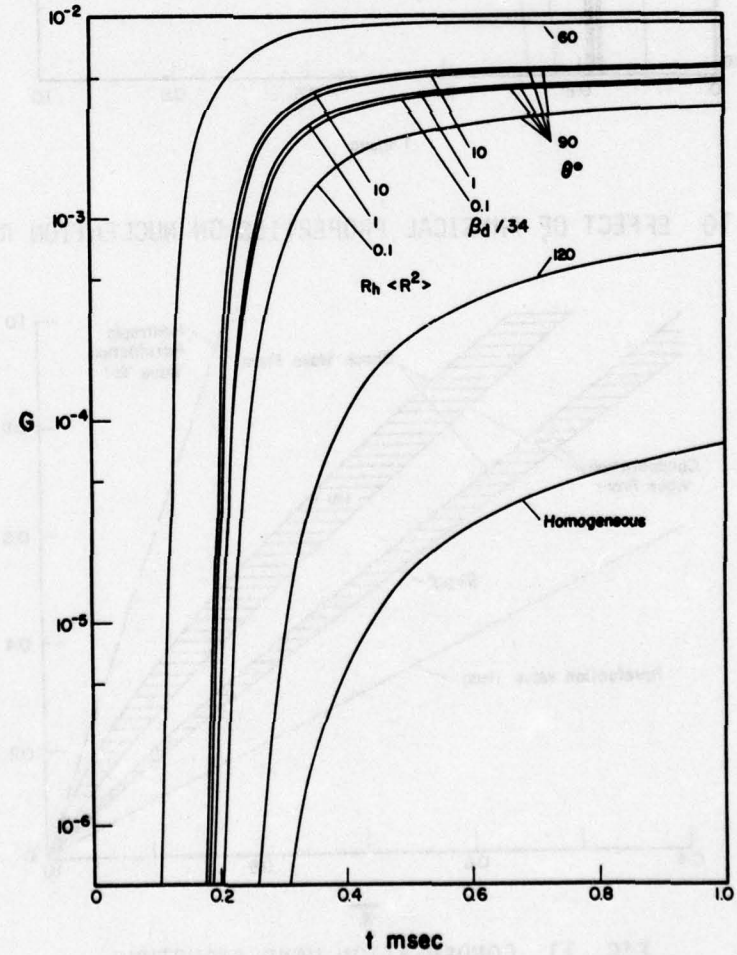

FIG. 9 EFFECT OF PHYSICAL PROPERTIES ON CONDENSATE MASS

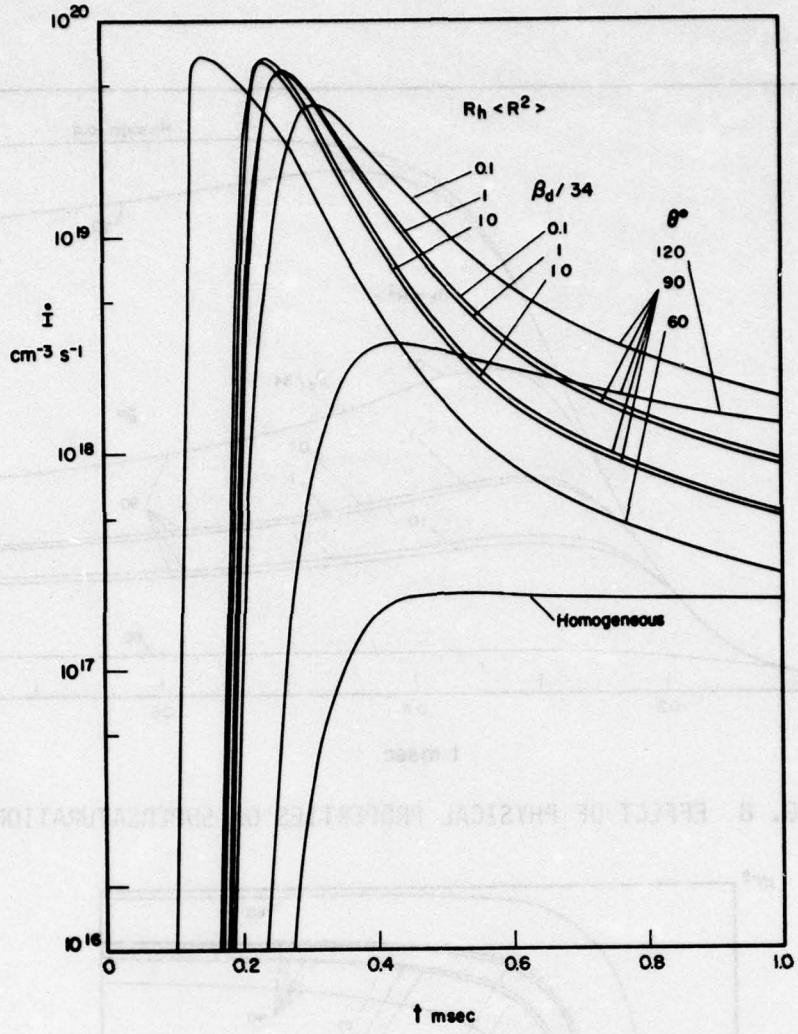

FIG. 10 EFFECT OF PHYSICAL PROPERTIES ON NUCLEATION RATE

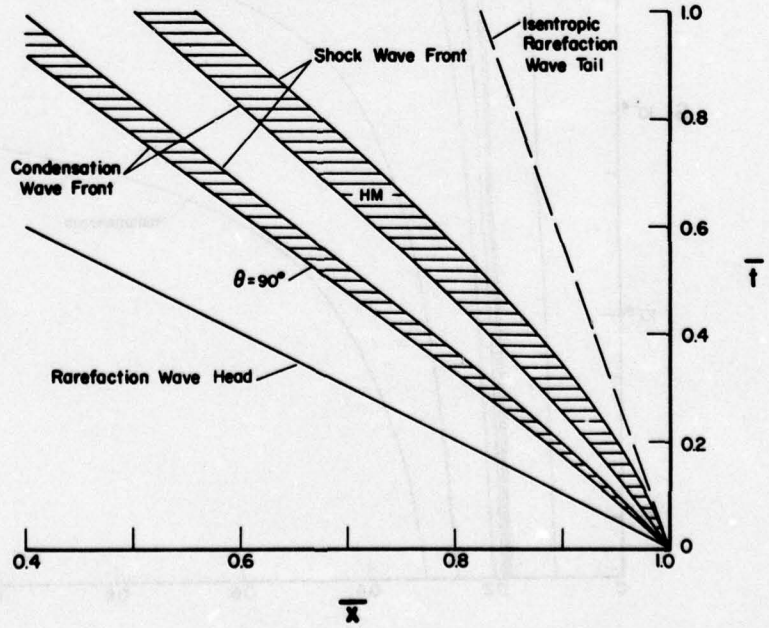

FIG. 11 CONDENSATION-WAVE STRUCTURE

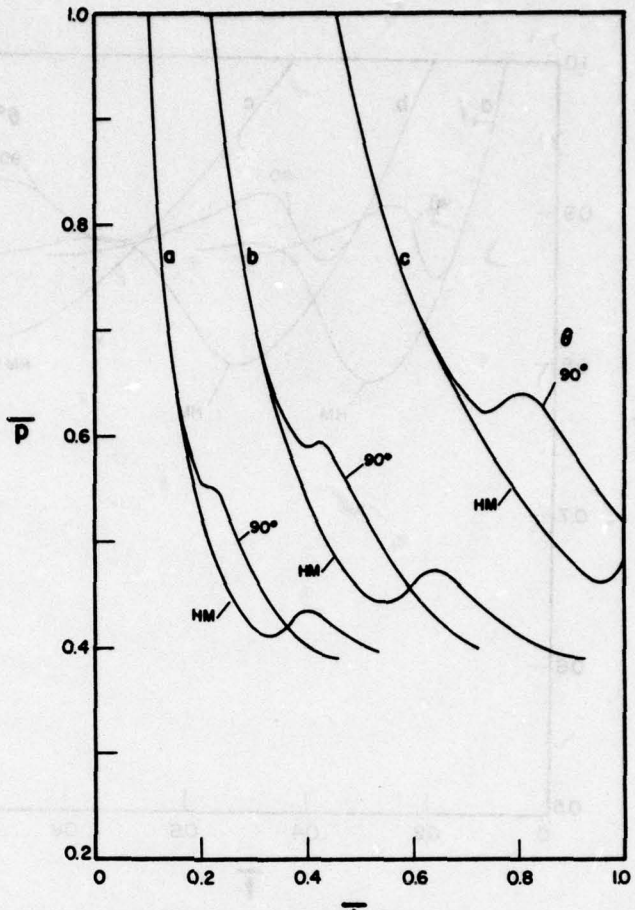

FIG. 12-a TIME-VARIATION OF PRESSURE ALONG PARTICLE PATHS INITIALLY AT -5(a), -10(b), -20(c) cm FROM THE DIAPHRAGM

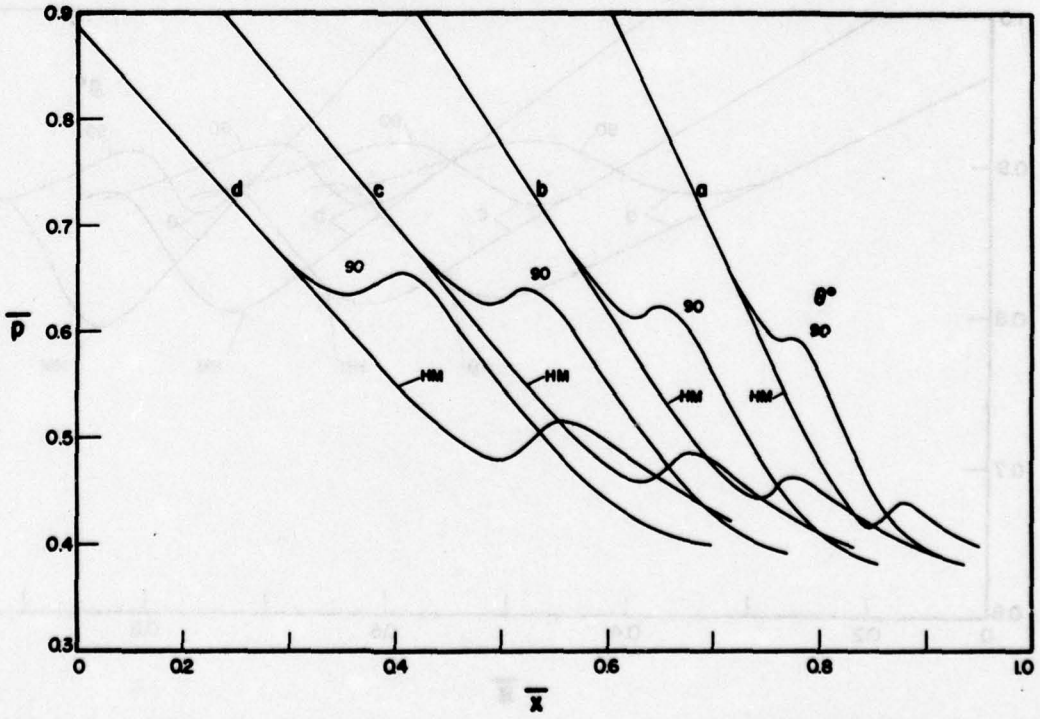

FIG. 12-b SPACE-VARIATION OF PRESSURE FOR TIME LEVELS; 0.48(a), 0.72(b), 0.96(c), 1.2(d) msec.

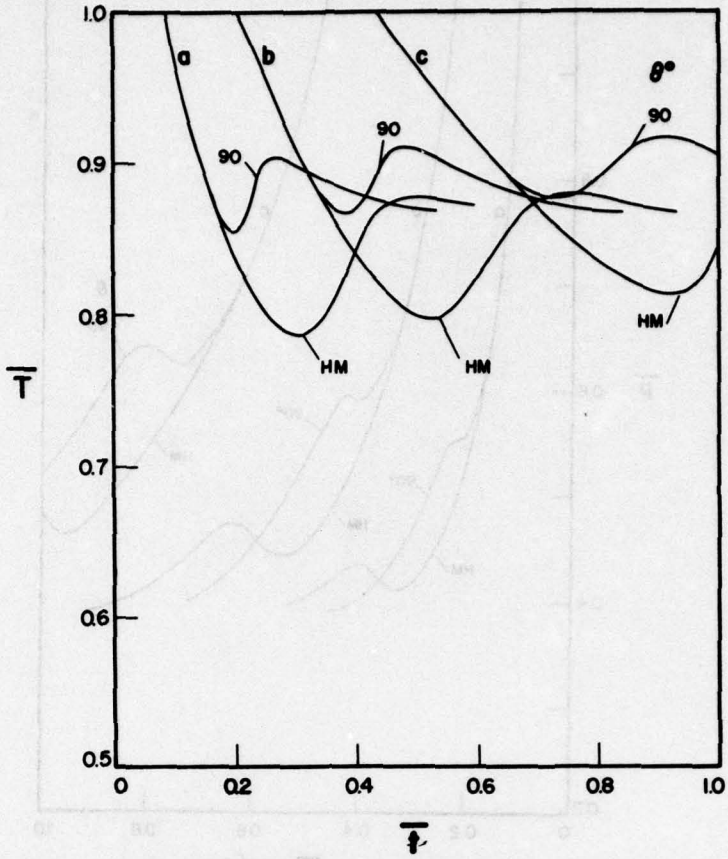

FIG. 13-a TIME-VARIATION OF TEMPERATURE ALONG PARTICLE PATHS INITIALLY AT -5(a), -10(b), -20(c), cm FROM THE DIAPHRAGM

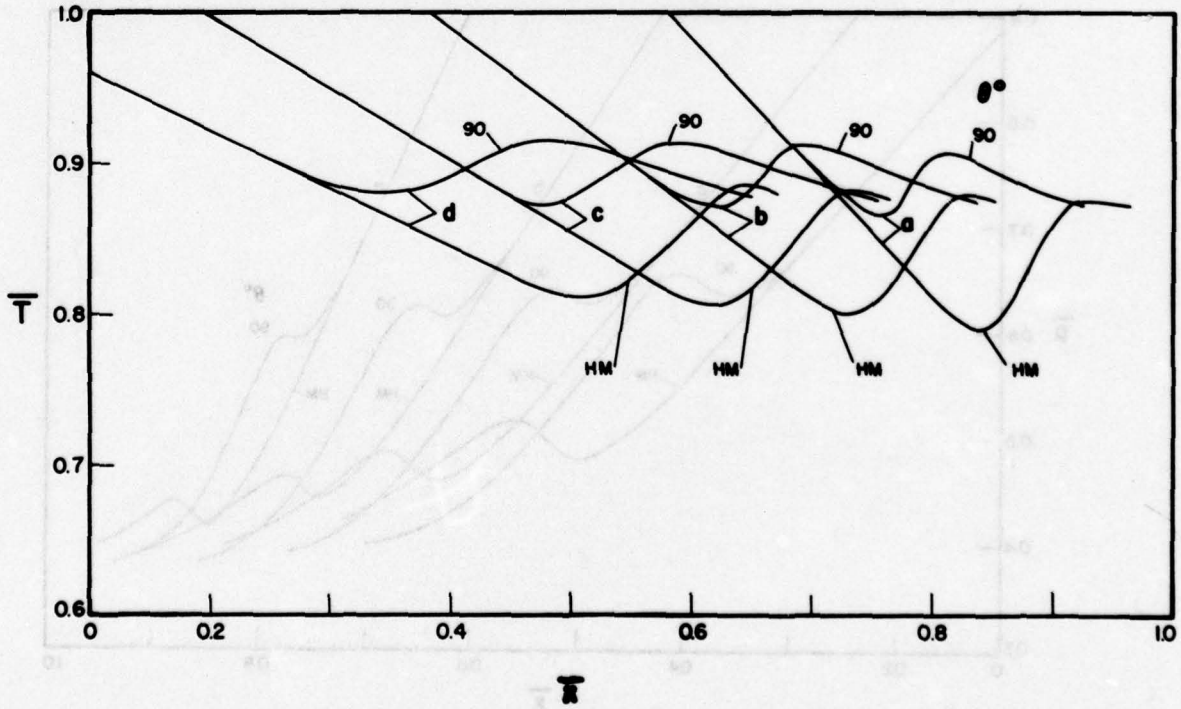

FIG. 13-b SPACE-VARIATION OF TEMPERATURE FOR TIME LEVELS; 0.48(a), 0.72(b), 0.96(c), 1.2(d) msec.

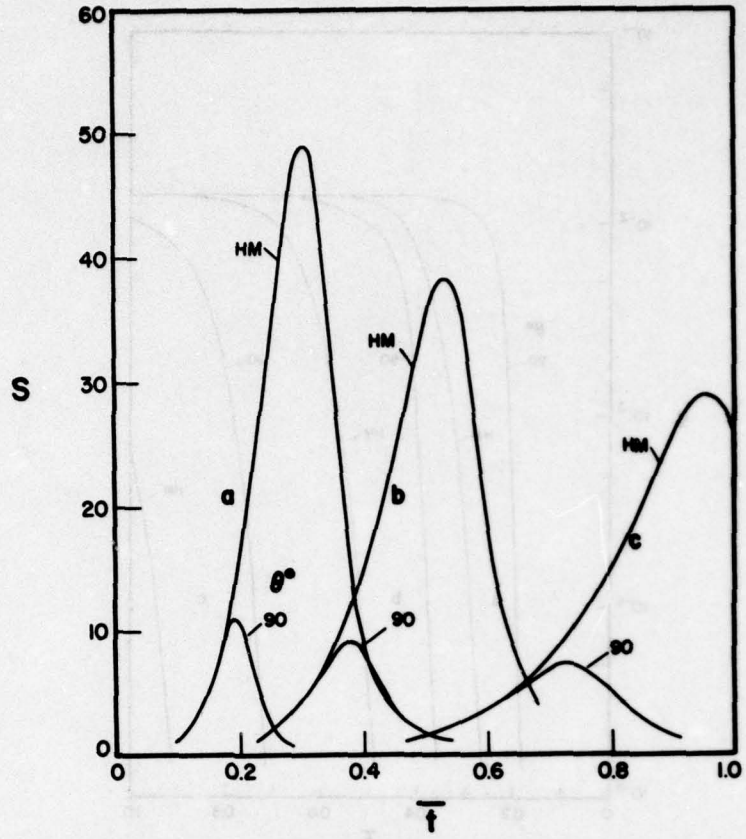

FIG. 14-a TIME-VARIATION OF SUPERSATURATION ALONG PARTICLE PATHS INITIALLY AT -5(a), -10(b), -20(c),cm FROM THE DIAPHRAGM

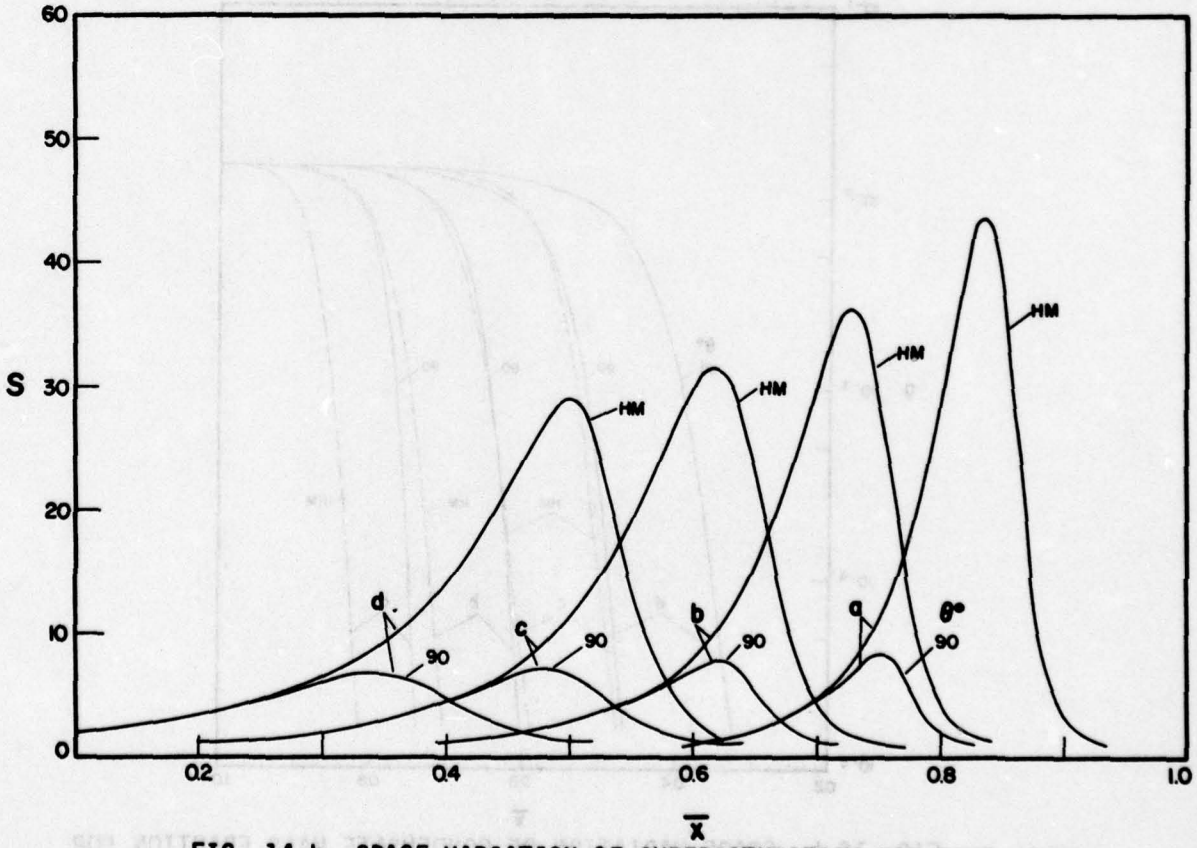

FIG. 14-b SPACE-VARIATION OF SUPERSATURATION FOR TIME LEVELS; 0.48(a), 0.72(b), 0.96(c), 1.2(d) msec.

FIG. 15-a TIME-VARIATION OF CONDENSATE MASS FRACTION ALONG PARTICLE PATHS INITIALLY AT -5(a), -10(b), -20(c), cm THE DIAPHRAGM

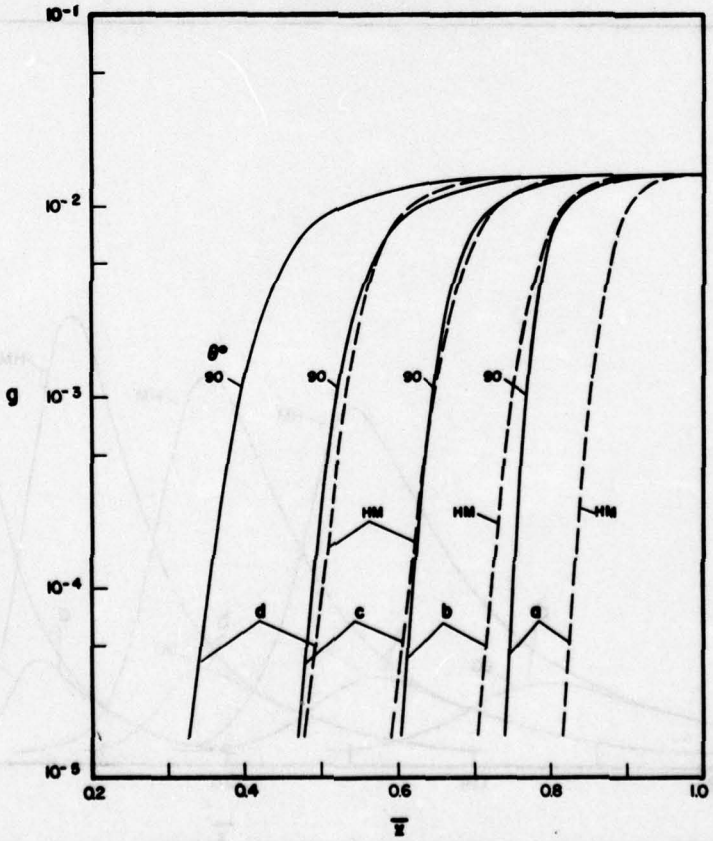

FIG. 15-b SPACE-VARIATION OF CONDENSATE MASS FRACTION FOR TIME LEVELS; 0.48(a), 0.72(b), 0.96(c), 1.2(d), msec.

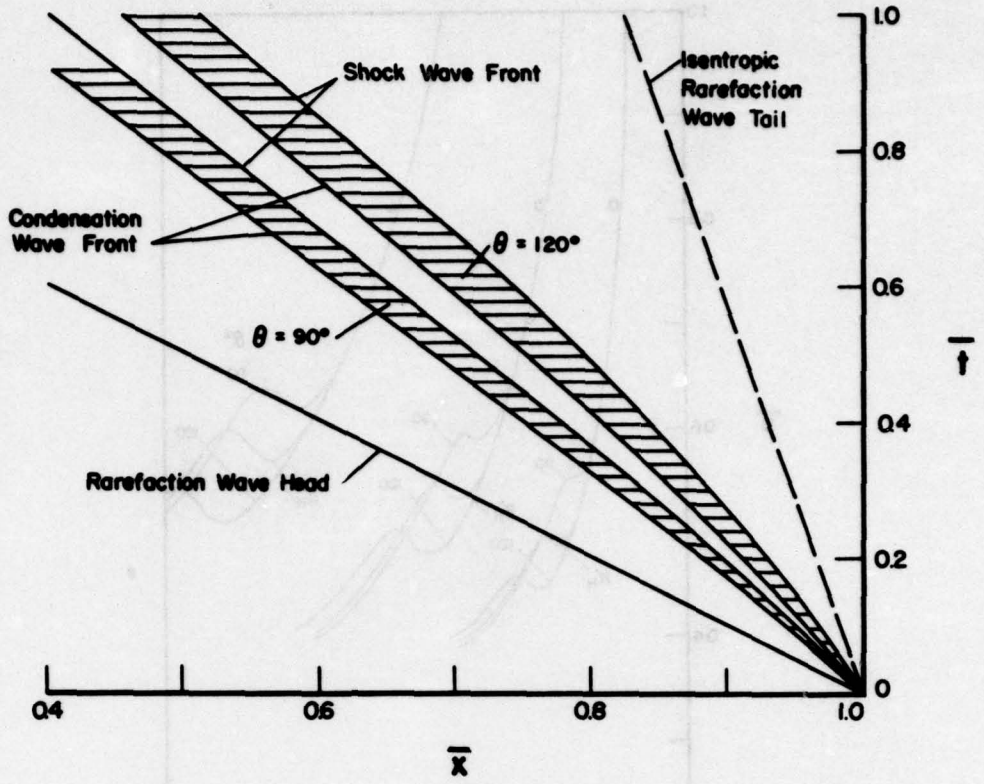

FIG. 16 CONDENSATION-WAVE STRUCTURE; EFFECT OF THE CONTACT ANGLE θ

(R_H = 0.311 x 10^6 cm)

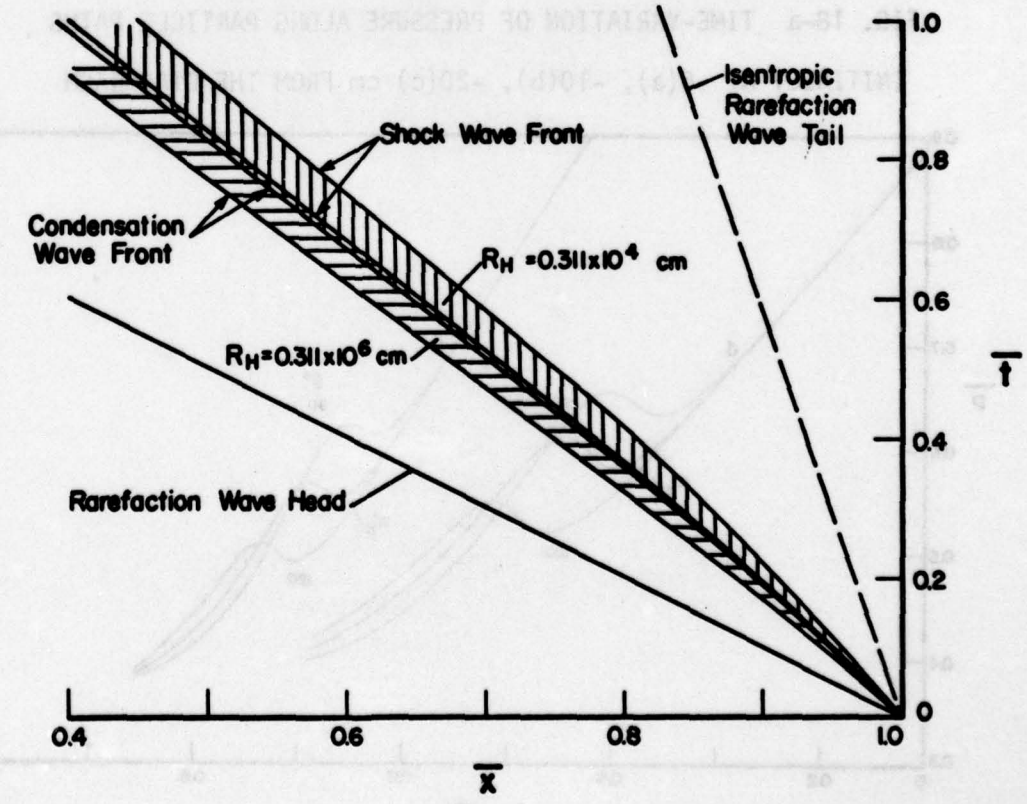

FIG. 17 CONDENSATION-WAVE STRACTURE; EFFECT OF THE FACTOR R_H (θ= 90°)

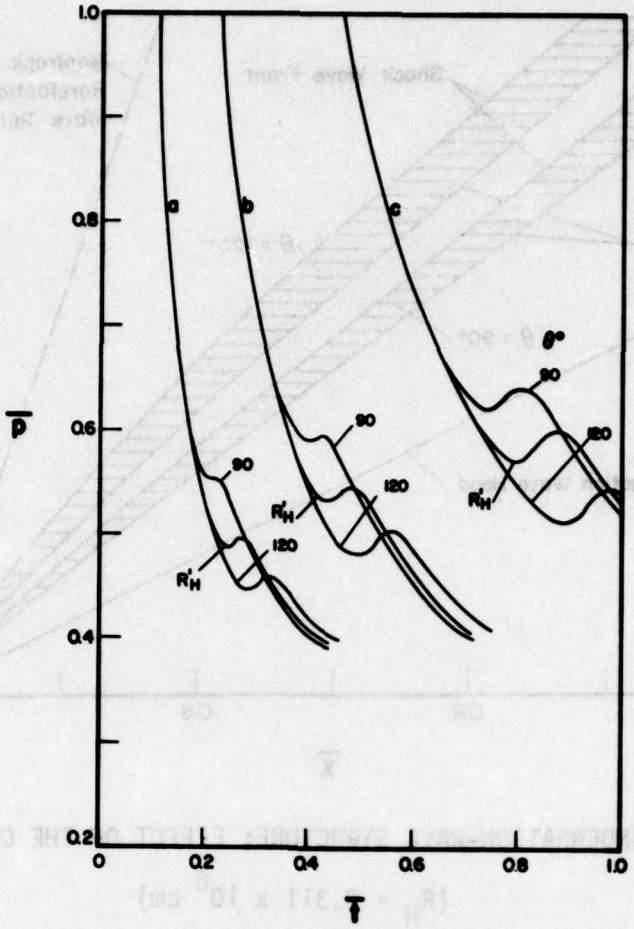

FIG. 18-a TIME-VARIATION OF PRESSURE ALONG PARTICLE PATHS INITIALLY AT -5(a), -10(b), -20(c) cm FROM THE DIAPHRAGM

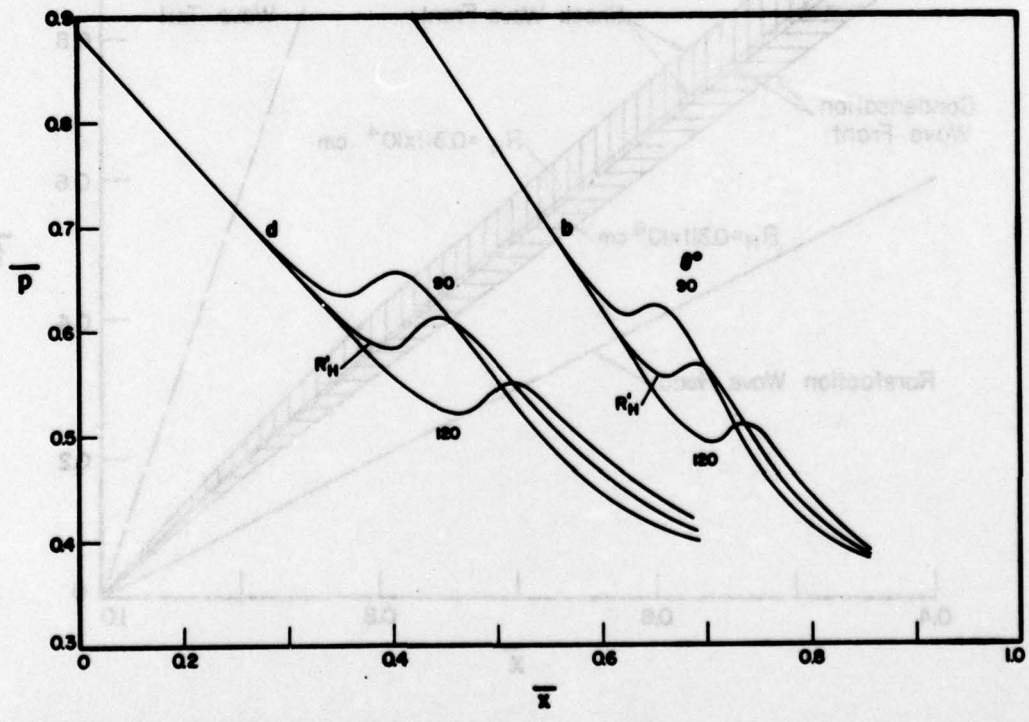

FIG. 18-b SPACE-VARIATION OF PRESSURE FOR TIME LEVELS; 0.72(b), 1.2(d) msec.

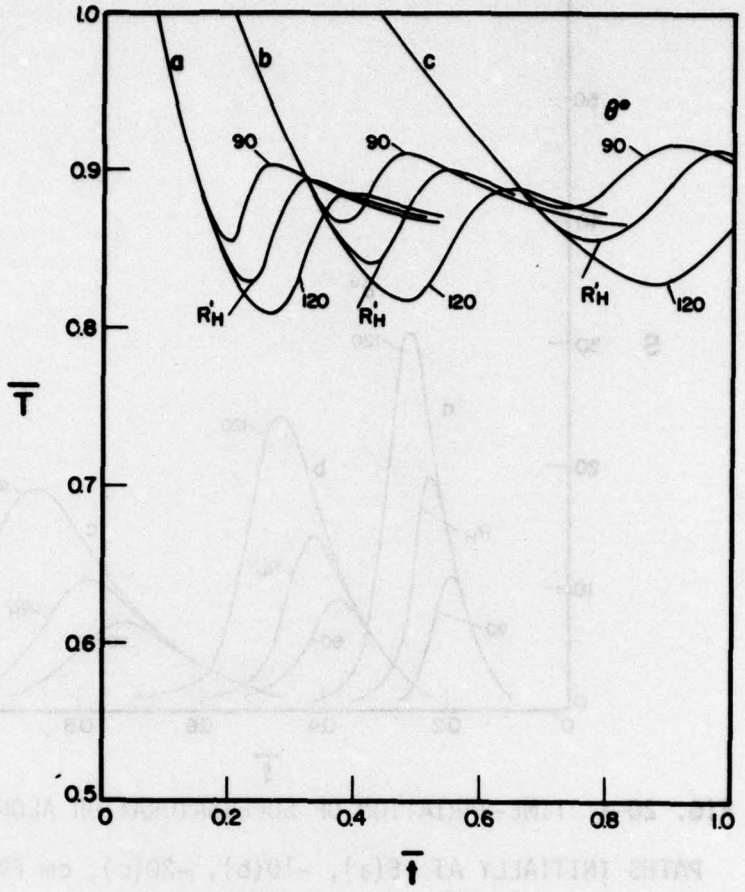

FIG. 19-a TIME-VARIATION OF TEMPERATURE ALONG PARTICLE PATHS INITIALLY AT -5(a), -10(b), -20(c), cm FROM THE DIAPHRAGM

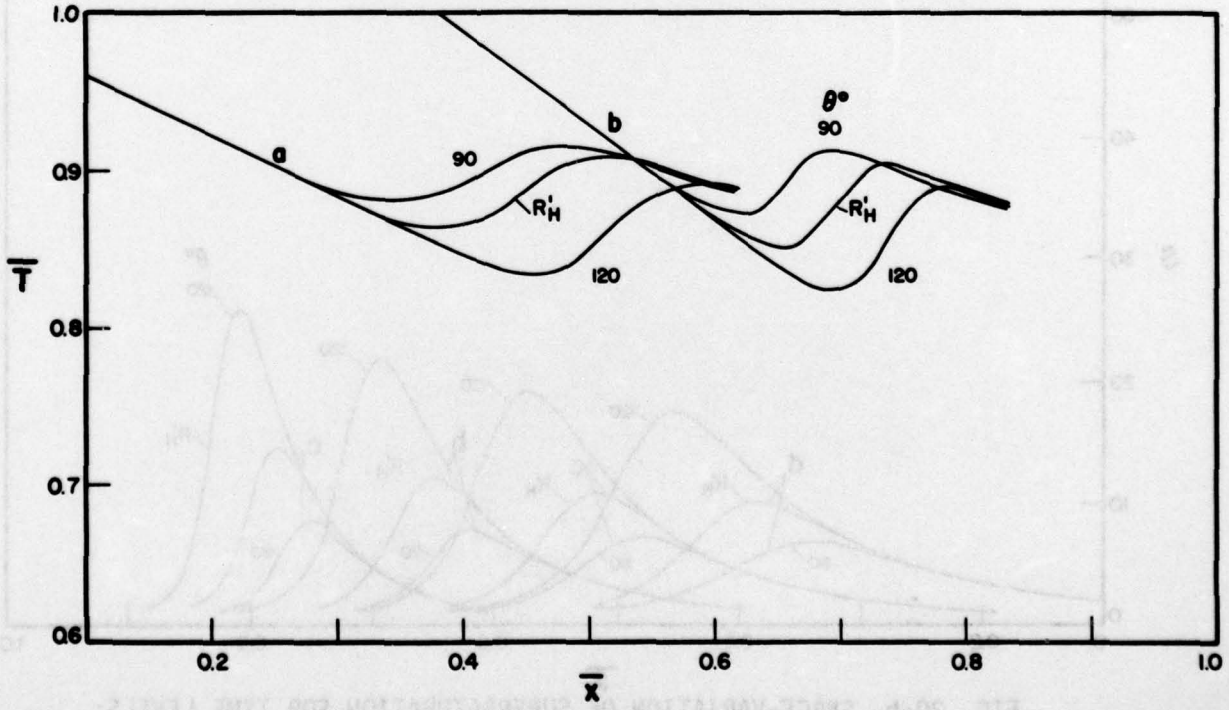

FIG. 19-b SPACE-VARIATION OF TEMPERATURE FOR TIME LEVELS; 0.72(b), 1.2(d) msec

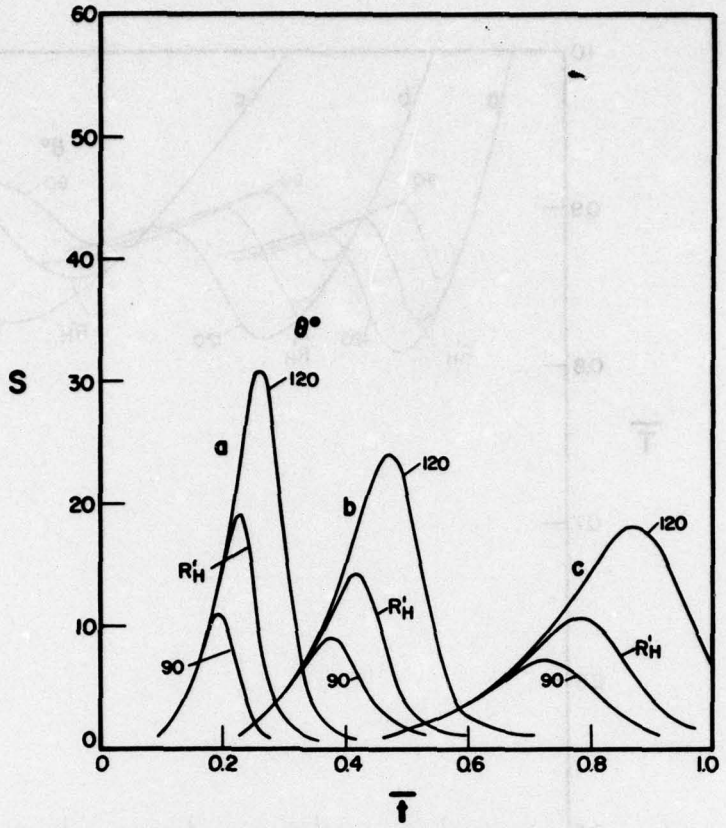

FIG. 20-a TIME-VARIATION OF SUPERSATURATION ALONG PARTICLE PATHS INITIALLY AT -5(a), -10(b), -20(c), cm FROM THE DIAPHRAGM

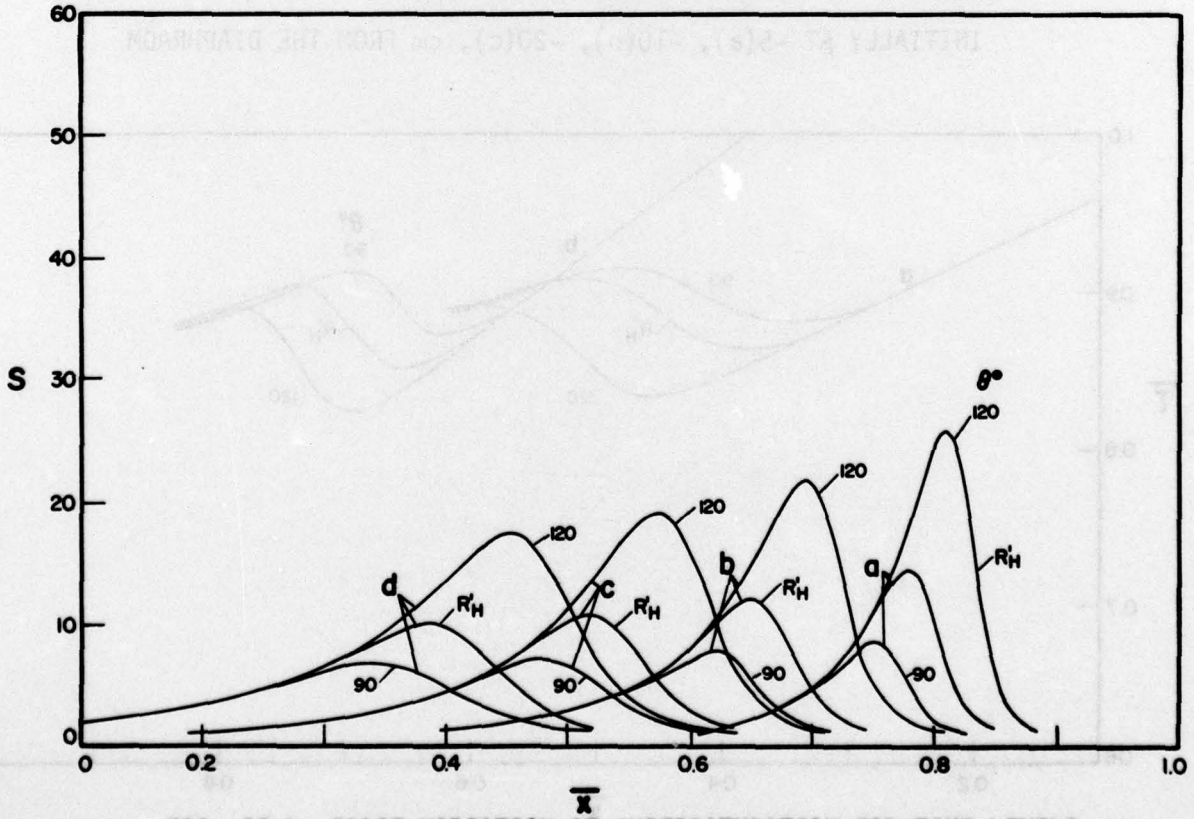

FIG. 20-b SPACE-VARIATION OF SUPERSATURATION FOR TIME LEVELS; 0.48(a), 0.72(b), 0.96(c), 1.2(d), msec.

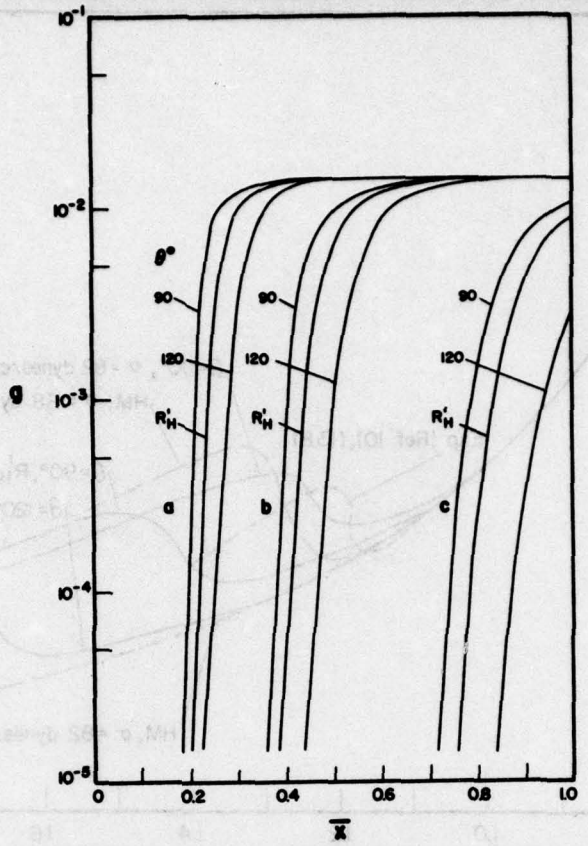

FIG. 21-a TIME-VARIATION OF CONDENSATE MASS FRACTION ALONG PARTICLE PATHS INITIALLY AT -5(a), -10(b), -20(c), cm FROM THE DIAPHRAGM

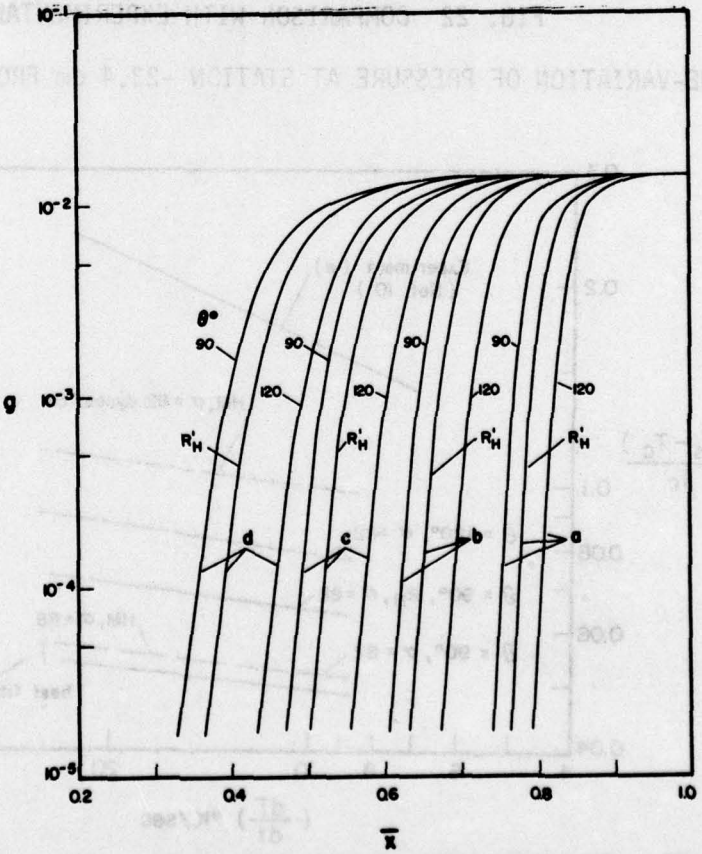

FIG. 21-b SPACE-VARIATION OF CONDENSATE MASS FRACTION FOR TIME LEVELS; 0.48(a), 0.72(b), 0.96(c), 1.2(d), msec.

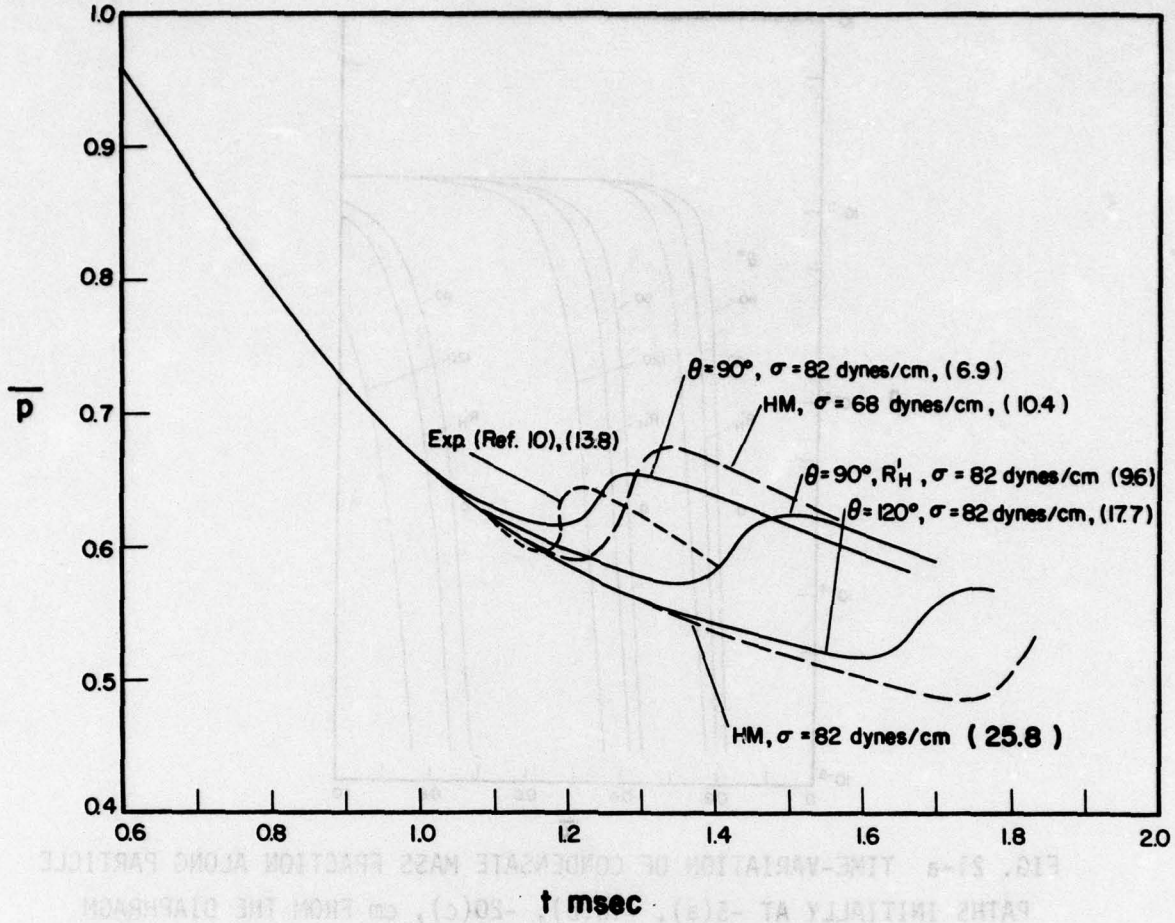

FIG. 22 COMPARISON WITH EXPERIMENTAL DATA;

TIME-VARIATION OF PRESSURE AT STATION -23.4 cm FROM THE DIAPHRAGM

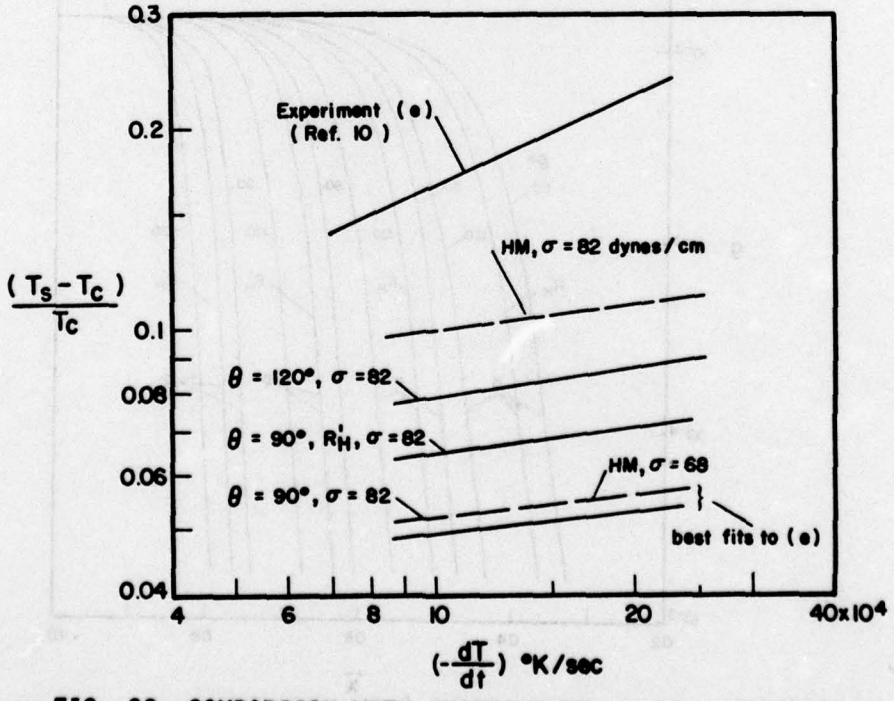

FIG. 23 COMPARISON WITH EXPERIMENTAL DATA; SUPERCOOLING VERSUS COOLING RATE

APPENDIX A: GEOMETRICAL PROPERTIES OF A CAP-SHAPED EMBRYO

Referring to Fig. 2, one obtains the geometrical properties of a cap-shaped embryo on the spherical surface of a solid particle as follows,

$$v_\ell = \frac{4}{3}\,\pi\, r^3\, a$$

$$a = \left\{1 - c_\theta\left(\cos\theta - \frac{r}{R}\right)\right\}^2 \left\{\frac{1}{2} + \frac{c_\theta}{4}\left(\cos\theta - \frac{r}{R}\right)\right\} \qquad \text{(A-1)}$$

$$- \left(\frac{R}{r}\right)^3 \left\{1 - c_\theta\left(1 - \frac{r}{R}\cos\theta\right)\right\}^2 \left\{\frac{1}{2} + \frac{c_\theta}{4}\left(1 - \frac{r}{R}\cos\theta\right)\right\}$$

Liquid-vapour surface area:

$$a_v = 4\pi\, r^2\, b_v$$

$$b_v = \frac{1}{2}\left\{1 - c_\theta\left(\cos\theta - \frac{r}{R}\right)\right\} \qquad \text{(A-2)}$$

Liquid-solid surface area:

$$a_s = 4\pi\, r^2\, b_s$$

$$b_s = \frac{1}{2}\left(\frac{R}{r}\right)^2 \left\{1 - c_\theta\left(1 - \frac{r}{R}\cos\theta\right)\right\} \qquad \text{(A-3)}$$

where

$$c_\theta = \left\{1 + \left(\frac{r}{R}\right)^2 - 2\,\frac{r}{R}\cos\theta\right\}^{-\frac{1}{2}}$$

The coefficients a, b_v and b_s are shown in Fig. 3 as a function of r/R. For r/R < 0.1, these coefficients take on almost constant values,

$$a_\infty = (1 - \cos\theta)^2\left(\frac{1}{2} + \frac{1}{4}\cos\theta\right)$$

$$b_{v\infty} = \frac{1}{2}(1 - \cos\theta) \qquad \text{(A-4)}$$

$$b_{s\infty} = \frac{1}{4}(1 - \cos^2\theta)$$

APPENDIX B: INTEGRATION OF RATE EQUATIONS

The rate of production of the liquid phase by heterogeneous nucleation and condensation is given by Eqs. 34,

$$\frac{dg}{dt} = \int_0^\infty \frac{\partial g_R}{\partial t} N(R)dR \tag{B-1}$$

$$\frac{\partial g_R}{\partial t} = \left\{ \frac{\dot{n}}{\rho} (A_o - A_s)\rho_\ell v_\ell^* \right\}_t + \int_0^t \left\{ \frac{\dot{n}}{\rho} (A_o - A_s) \frac{\partial}{\partial t} (\rho_\ell v_\ell) \right\}_\tau d\tau \tag{B-2}$$

where, the surface area of a nucleus, wetted by condensate droplets, A_s is given by,

$$\frac{\partial A_s}{\partial t} = \{\dot{n}(A_o - A_s)a_s^*\}_t + \int_0^t \left\{ \dot{n}(A_o - A_s) \frac{\partial a_s}{\partial t} \right\}_\tau d\tau \tag{B-3}$$

The liquid-solid interfacial area of a condensate droplet nucleated at time τ is given by,

$$a_s(\tau,t) = a_s^*(\tau) + \int_\tau^t \dot{a}_s(\tau)d\tau' \tag{B-4}$$

where, $\dot{a}_s$ is the growth rate of the liquid-solid surface area.

For the numerical integration of these equations, it is possible to reduce them to a set of differential equations. Successive differentiation of Eq. B-2 with respect to time leads to,

$$\begin{aligned}
\frac{\partial g_R}{\partial t} &= 4\pi \rho_\ell \left\{ (A_o - A_s) \frac{\dot{n}}{\rho} \frac{r^{*3}}{3} a + \dot{r}_o A \right\} \\
\frac{\partial A}{\partial t} &= \frac{\dot{n}}{\rho} (A_o - A_s) r^{*2} b_v + \dot{r}_o B \\
\frac{\partial B}{\partial t} &= \frac{\dot{n}}{\rho} (A_o - A_s) r^* c_b + \dot{r}_o C \\
\frac{\partial C}{\partial t} &= \frac{\dot{n}}{\rho} (A_o - A_s) c_c + \dot{r}_o C_1 \\
\frac{\partial C_1}{\partial t} &= \frac{\dot{n}}{\rho} (A_o - A_s) c_{c1} + \dot{r}_o C_2 \\
\frac{\partial C_2}{\partial t} &= \frac{\dot{n}}{\rho} (A_o - A_s) c_{c2} + \dot{r}_o C_3 \\
&\cdots\cdots\cdots
\end{aligned} \tag{B-5}$$

where,

$$A \equiv \int_o^t \frac{\dot{n}}{\rho} (A_o - A_s)\, r(\tau,t)^2\, b_v\, d\tau$$

$$B \equiv \int_o^t \frac{\dot{n}}{\rho} (A_o - A_s)\, r(\tau,t)\, c_b\, d\tau$$

$$C \equiv \int_o^t \frac{\dot{n}}{\rho} (A_o - A_s)\, c_c\, d\tau \qquad \text{(B-6)}$$

$$C_1 \equiv \int_o^t \frac{\dot{n}}{\rho} (A_o - A_s)\, c_{c1}\, d\tau$$

$$C_2 \equiv \int_o^t \frac{\dot{n}}{\rho} (A_o - A_s)\, c_{c2}\, d\tau$$

.....

$$c_b = \frac{\dot{r}}{\dot{r}_o} \frac{\partial}{\partial r} (r^2 b_v) = K \cdot 2 \left(b_v + \frac{r}{2} \frac{\partial b_v}{\partial r} \right)$$

$$= K \left\{ 1 - c_\theta \left(\cos\theta - \frac{r}{R}\right) + \frac{c_\theta^3}{2} \frac{r}{R} (1 - \cos^2\theta) \right\}$$

$$c_c = K \frac{\partial (r c_b)}{\partial r} \qquad \text{(B-7)}$$

$$c_{c1} = K \frac{\partial c_c}{\partial r}$$

$$c_{c2} = K \frac{\partial c_{c1}}{\partial r}$$

.....

where

$$K = \frac{\dot{r}}{\dot{r}_o} = \frac{b_v}{a} \left(1 + \frac{r}{3a} \frac{\partial a}{\partial r} \right)^{-1}$$

$$= \frac{1}{2} \left\{ 1 - c_\theta \left(\cos\theta - \frac{r}{R} \right) \right\} \left[\left\{ 1 - c_\theta \left(\cos\theta - \frac{r}{R} \right) \right\}^2 \left\{ \frac{1}{2} + \frac{c_\theta}{4} \left(\cos\theta - \frac{r}{R} \right) \right\} \right.$$

$$\left. + \frac{c_\theta^5}{2} \frac{r}{R} \cos\theta (1 - \cos\theta)(1 - \cos^2\theta) \right]^{-1} \qquad \text{(B-8)}$$

When c_{cn} hardly changes with respect to r or r/R,

$$C_{n+1} = \int_0^t \frac{\dot{n}}{\rho} (A_o - A_s) K \frac{\partial c_{cn}}{\partial r} d\tau \simeq 0$$

which leads to

$$\frac{\partial C_n}{\partial t} = \frac{\dot{n}}{\rho} (A_o - A_s) c_{cn}$$

The integral equation can be replaced then by sequential ordinary differential equations in a closed form.

Similarly, the integral equation of the wetted surface area of a nucleus (B-3) can be reduced to the following sequence of ordinary differential equations,

$$\begin{aligned}
\frac{\partial A_s}{\partial t} &= \dot{n}(A_o - A_s)\, 4\pi r^{*2}\, b_s + \dot{r}_o\, B_s \\
\frac{\partial B_s}{\partial t} &= \dot{n}(A_o - A_s)\, 2\pi r^*\, \dot{c}_{sb} + \dot{r}_o\, C_s \\
\frac{\partial C_s}{\partial t} &= \dot{n}(A_o - A_s)\, 2\pi\, c_{sc} + \dot{r}_o\, C_{s1} \\
\frac{\partial C_{s1}}{\partial t} &= \dot{n}(A_o - A_s)\, 2\pi\, c_{sc1} + \dot{r}_o\, C_{s2} \\
\frac{\partial C_{s2}}{\partial t} &= \dot{n}(A_o - A_s)\, 2\pi\, c_{sc2} + \dot{r}_o\, C_{s3} \\
&\cdots\cdots\cdots
\end{aligned} \tag{B-9}$$

where

$$\begin{aligned}
B_s &\equiv \int_0^t \dot{n}(A_o - A_s)\, r\, c_{sb}\, d\tau \\
C_s &\equiv \int_0^t \dot{n}(A_o - A_s)\, c_{sc}\, d\tau \\
C_{s1} &\equiv \int_0^t \dot{n}(A_o - A_s)\, c_{sc1}\, d\tau \\
C_{s2} &\equiv \int_0^t \dot{n}(A_o - A_s)\, c_{sc2}\, d\tau \\
&\cdots\cdots\cdots
\end{aligned} \tag{B-10}$$

$$c_{sb} = \frac{\dot{r}}{r\,\dot{r}_o} \frac{\partial}{\partial r} (4\pi r^2 b_s) = \frac{2\pi}{c_\theta^3} (1 - \cos^2\theta)K$$

$$c_{sc} = K \frac{\partial}{\partial r} (r\, c_{sb})$$

$$c_{sc1} = K \frac{\partial c_{sc}}{\partial r} \qquad \text{(B-11)}$$

$$c_{sc2} = K \frac{\partial c_{sc1}}{\partial r}$$

.....

When c_{scn} takes on almost constant values with respect to r or r/R,

$$C_{s,n+1} = \int_o^t \dot{n}(A_o - A_s)\, K \frac{\partial c_{scn}}{\partial r}\, d\tau \simeq 0$$

which yields,

$$\frac{\partial C_{sn}}{\partial t} = \dot{n}(A_o - A_s)\, 2\pi\, c_{sn}$$

It means that the integral equation (B-3) can be explicitly replaced by a set of ordinary differential equations.

In Fig. 5 are shown the coefficients K, c_b, cc, c_{sb} and c_{sc} which are approximately constant for $r/R < 0.1$, taking the following values:

$$c_{b\infty} = \frac{2}{2 + \cos\theta}$$

$$c_{c\infty} = K_\infty\, c_{b\infty}$$

$$c_{c1\infty} = 0$$

$$c_{sb\infty} = (1 - \cos^2\theta) \qquad \text{(B-12)}$$

$$c_{sc\infty} = K_\infty\, c_{sb\infty}$$

$$c_{sc1\infty} = 0$$

$$K_\infty = \frac{1}{2}\left\{(1 + \cos\theta)\left(\frac{1}{2} + \frac{1}{4}\cos\theta\right)\right\}^{-1}$$

In this case, the differential equations can be written as follows:

$$\frac{dg_R}{dt} = 4\pi \rho_\ell \left\{ \frac{\dot{n}}{\rho} (1 - \bar{A}_s) \frac{r^{*3}}{3} a_\infty + \dot{r}_o A \right\}$$

$$\frac{dA}{dt} = \frac{\dot{n}}{\rho} (1 - \bar{A}_s) r^{*2} b_{v\infty} + \dot{r}_o B$$

$$\frac{dB}{dt} = \frac{\dot{n}}{\rho} (1 - \bar{A}_s) r^{*} c_{b\infty} + \dot{r}_o C$$

$$\frac{dC}{dt} = \frac{\dot{n}}{\rho} (1 - \bar{A}_s) c_{c\infty} \qquad \text{(B-13)}$$

$$\frac{d\bar{A}_s}{dt} = \dot{n}(1 - \bar{A}_s) 4\pi r^{*2} b_{s\infty} + \dot{r}_o \bar{B}_s$$

$$\frac{d\bar{B}_s}{dt} = \dot{n}(1 - \bar{A}_s) 2\pi r^{*} c_{sb\infty} + \dot{r}_o \bar{C}_s$$

$$\frac{d\bar{C}_s}{dt} = \dot{n}(1 - \bar{A}_s) 2\pi c_{sc\infty}$$

where, g_R, A, B,... mean g_R, A, B,... divided by A_o which is equal to $4\pi R^2$. The rate of production of overall condensate mass fraction is then given by,

$$\frac{dg}{dt} = \int_o^\infty \frac{\partial g_R}{\partial t} 4\pi R^2 N(R) dR = \frac{dg_R}{dt} \int_o^\infty 4\pi R^2 N(R) dR \qquad \text{(B-14)}$$

UTIAS REPORT NO. 207

Institute for Aerospace Studies, University of Toronto

CONDENSATION OF WATER VAPOUR ON HETEROGENEOUS NUCLEI IN A SHOCK TUBE

Kotake, S. and Glass, I. I.   40 pages   23 figures

1. Condensation shock waves   2. Rarefaction waves   3. Heterogeneos nucleation
4. Two-phase flows   5. Nonequilibrium flows   6. Shock tubes

I. Kotake, S., Glass, I. I.   II. UTIAS Report No. 207

A macroscopic model of heterogeneous nucleation is used for a theoretical study of condensation of water vapour/carrier gas mixtures in a nonequilibrium nonstationary rarefaction wave generated in a shock tube. The results are compared with those from homogeneous nucleation. Nucleation is assumed to take place heterogeneously on idealized smooth, spherical solid particles of Aitken nuclei, which are chemically and electrically inert. In the processes of heterogeneous condensation, the controlling factors are the size-distribution of nuclei, the concentration of monomers on the surface of the substrate and the contact angle of embryos. Of these factors the most dominant is the contact angle, which can reduce greatly the activation energy of nucleation. Heterogeneous condensation results in less supercooling of the mixture but a faster approach to the equilibrium state. By choosing a suitable value for the contact angle, the numerical results can be made to fit the experimental data. Although this is not entirely satisfactory, it is probably preferable to changing the value of surface tension as in the homogeneous nucleation case in order to obtain agreement with experimental results.

Available copies of this report are limited. Return this card to UTIAS, if you require a copy.

UTIAS REPORT NO. 207

Institute for Aerospace Studies, University of Toronto

CONDENSATION OF WATER VAPOUR ON HETEROGENEOUS NUCLEI IN A SHOCK TUBE

Kotake, S. and Glass, I. I.   40 pages   23 figures

1. Condensation shock waves   2. Rarefaction waves   3. Heterogeneos nucleation
4. Two-phase flows   5. Nonequilibrium flows   6. Shock tubes

I. Kotake, S., Glass, I. I.   II. UTIAS Report No. 207

A macroscopic model of heterogeneous nucleation is used for a theoretical study of condensation of water vapour/carrier gas mixtures in a nonequilibrium nonstationary rarefaction wave generated in a shock tube. The results are compared with those from homogeneous nucleation. Nucleation is assumed to take place heterogeneously on idealized smooth, spherical solid particles of Aitken nuclei, which are chemically and electrically inert. In the processes of heterogeneous condensation, the controlling factors are the size-distribution of nuclei, the concentration of monomers on the surface of the substrate and the contact angle of embryos. Of these factors the most dominant is the contact angle, which can reduce greatly the activation energy of nucleation. Heterogeneous condensation results in less supercooling of the mixture but a faster approach to the equilibrium state. By choosing a suitable value for the contact angle, the numerical results can be made to fit the experimental data. Although this is not entirely satisfactory, it is probably preferable to changing the value of surface tension as in the homogeneous nucleation case in order to obtain agreement with experimental results.

Available copies of this report are limited. Return this card to UTIAS, if you require a copy.

UTIAS REPORT NO. 207

Institute for Aerospace Studies, University of Toronto

CONDENSATION OF WATER VAPOUR ON HETEROGENEOUS NUCLEI IN A SHOCK TUBE

Kotake, S. and Glass, I. I.   40 pages   23 figures

1. Condensation shock waves   2. Rarefaction waves   3. Heterogeneos nucleation
4. Two-phase flows   5. Nonequilibrium flows   6. Shock tubes

I. Kotake, S., Glass, I. I.   II. UTIAS Report No. 207

A macroscopic model of heterogeneous nucleation is used for a theoretical study of condensation of water vapour/carrier gas mixtures in a nonequilibrium nonstationary rarefaction wave generated in a shock tube. The results are compared with those from homogeneous nucleation. Nucleation is assumed to take place heterogeneously on idealized smooth, spherical solid particles of Aitken nuclei, which are chemically and electrically inert. In the processes of heterogeneous condensation, the controlling factors are the size-distribution of nuclei, the concentration of monomers on the surface of the substrate and the contact angle of embryos. Of these factors the most dominant is the contact angle, which can reduce greatly the activation energy of nucleation. Heterogeneous condensation results in less supercooling of the mixture but a faster approach to the equilibrium state. By choosing a suitable value for the contact angle, the numerical results can be made to fit the experimental data. Although this is not entirely satisfactory, it is probably preferable to changing the value of surface tension as in the homogeneous nucleation case in order to obtain agreement with experimental results.

Available copies of this report are limited. Return this card to UTIAS, if you require a copy.

UTIAS REPORT NO. 207

Institute for Aerospace Studies, University of Toronto

CONDENSATION OF WATER VAPOUR ON HETEROGENEOUS NUCLEI IN A SHOCK TUBE

Kotake, S. and Glass, I. I.   40 pages   23 figures

1. Condensation shock waves   2. Rarefaction waves   3. Heterogeneos nucleation
4. Two-phase flows   5. Nonequilibrium flows   6. Shock tubes

I. Kotake, S., Glass, I. I.   II. UTIAS Report No. 207

A macroscopic model of heterogeneous nucleation is used for a theoretical study of condensation of water vapour/carrier gas mixtures in a nonequilibrium nonstationary rarefaction wave generated in a shock tube. The results are compared with those from homogeneous nucleation. Nucleation is assumed to take place heterogeneously on idealized smooth, spherical solid particles of Aitken nuclei, which are chemically and electrically inert. In the processes of heterogeneous condensation, the controlling factors are the size-distribution of nuclei, the concentration of monomers on the surface of the substrate and the contact angle of embryos. Of these factors the most dominant is the contact angle, which can reduce greatly the activation energy of nucleation. Heterogeneous condensation results in less supercooling of the mixture but a faster approach to the equilibrium state. By choosing a suitable value for the contact angle, the numerical results can be made to fit the experimental data. Although this is not entirely satisfactory, it is probably preferable to changing the value of surface tension as in the homogeneous nucleation case in order to obtain agreement with experimental results.

Available copies of this report are limited. Return this card to UTIAS, if you require a copy.

UNCLASSIFIED

SECURITY CLASSIFICATION OF THIS PAGE (When Data Entered)

REPORT DOCUMENTATION PAGE

READ INSTRUCTIONS BEFORE COMPLETING FORM

1. REPORT NUMBER: AFOSR - TR-77-0039	2. GOVT ACCESSION NO.
3. RECIPIENT'S CATALOG NUMBER	
4. TITLE (and Subtitle): CONDENSATION OF WATER VAPOUR ON HETEROGENEOUS NUCLEI IN A SHOCK TUBE	5. TYPE OF REPORT & PERIOD COVERED: INTERIM
	6. PERFORMING ORG. REPORT NUMBER: REPORT NO. 207
7. AUTHOR(s): S. Kotake and I. I. Glass	8. CONTRACT OR GRANT NUMBER(s): AFOSR 72-2274
9. PERFORMING ORGANIZATION NAME AND ADDRESS: University of Toronto, Institute for Aerospace Studies, 4925 Dufferin St., Downsview, Ontario, Canada, M3H 5T6	10. PROGRAM ELEMENT, PROJECT, TASK AREA & WORK UNIT NUMBERS: 11 Apr 76
11. CONTROLLING OFFICE NAME AND ADDRESS: Air Force Office of Scientific Research, Bolling Air Force Base, Bldg. 410, Washington, D.C. 20332, U.S.A.	12. REPORT DATE
	13. NUMBER OF PAGES: 40
14. MONITORING AGENCY NAME & ADDRESS (if different from Controlling Office): 12 59p.	15. SECURITY CLASS. (of this report): UNCLASSIFIED
	15a. DECLASSIFICATION/DOWNGRADING SCHEDULE

16. DISTRIBUTION STATEMENT (of this Report)

Approved for public release; distribution unlimited.

17. DISTRIBUTION STATEMENT (of the abstract entered in Block 20, if different from Report)

14 UTIAS-207

18. SUPPLEMENTARY NOTES

15 AF-AFOSR-2274-72

19. KEY WORDS (Continue on reverse side if necessary and identify by block number)

1. Condensation shock waves, 2. Rarefaction waves, 3. Heterogeneous nucleation, 4. Two-phase flows, 5. Nonequilibrium flows, 6. Shock tubes

20. ABSTRACT (Continue on reverse side if necessary and identify by block number)

A macroscopic model of heterogeneous nucleation is used for a theoretical study of condensation of water vapour/carrier gas mixtures in a nonequilibrium nonstationary rarefaction wave generated in a shock tube. The results are compared with those from homogeneous nucleation. Nucleation is assumed to take place heterogeneously on idealized smooth, spherical solid particles of Aitken nuclei, which are chemically and electrically inert. In the processes of heterogeneous condensation, the controlling factors are the size-distribution

DD FORM 1 JAN 73 1473 EDITION OF 1 NOV 65 IS OBSOLETE

UNCLASSIFIED

SECURITY CLASSIFICATION OF THIS PAGE (When Data Entered)

178920

of nuclei, the concentration of monomers on the surface of the substrate and the contact angle of embryos. Of these factors the most dominant is the contact angle, which can reduce greatly the activation energy of nucleation. Heterogeneous condensation results in less supercooling of the mixture but a faster approach to the equilibrium state. By choosing a suitable value for the contact angle, the numerical results can be made to fit the experimental data. Although this is not entirely satisfactory, it is probably preferable to changing the value of surface tension as in the homogeneous nucleation case in order to obtain agreement with experimental results.